CERAMIC LIFE PREDICTION METHODOLOGY FINAL REPORT

L.R. SWANK, J.A. MANGELS
J.C. CAVERLY, R.K. GOVILA

Research Staff
Ford Motor Company
P.O. Box 2053
Dearborn, Michigan 48121

May 1986

Contract No. DAAG 46-77-C-0023
Prepared for
U.S. ARMY MATERIALS TECHNOLOGY LABORATORY
WATERTOWN, MASSACHUSETTS 02172-0001

U.S. DEPARTMENT OF ENERGY

Division of Transportation Energy Conservation

The findings in this report are not to be construed as an official Department of the Army position, unless so designated by other authorized documents.

Mention of any trade names or manufacturers in this report shall not be construed as advertising nor as an official indorsement or approval of such products or companies by the United States Government.

DISPOSITION INSTRUCTIONS

Destroy this report when it is no longer needed.
Do not return it to the originator.

UNCLASSIFIED

SECURITY CLASSIFICATION OF THIS PAGE *(When Data Entered)*

REPORT DOCUMENTATION PAGE		READ INSTRUCTIONS BEFORE COMPLETING FORM
1. REPORT NUMBER MTL 86 - 16	2. GOVT ACCESSION NO.	3 RECIPIENT'S CATALOG NUMBER
4. TITLE *(and Subtitle)* Ceramic Life Prediction Methodology - Final Report		5. TYPE OF REPORT & PERIOD COVERED Final 1 Jan 83 to 31 Dec 85
		6 PERFORMING ORG. REPORT NUMBER
7. AUTHOR(s) L. R. Swank, J.A Mangels, J.C. Caverly and R. K. Govila		8 CONTRACT OR GRANT NUMBER(s) DAAG-77-C-0028
9. PERFORMING ORGANIZATION NAME AND ADDRESS Ford Motor Company Room E-3172 SRL, P.O. Box 2053 Dearborn, Michigan 48121		10. PROGRAM ELEMENT, PROJECT, TASK AREA & WORK UNIT NUMBERS DOE IA No:DE-AI05-840R 21411
11. CONTROLLING OFFICE NAME AND ADDRESS Army Materials Technology Laboratory Attn: SLCMT-ISC Watertown, Massachusetts 02172		12. REPORT DATE May 1986 13. NUMBER OF PAGES 69
14. MONITORING AGENCY NAME & ADDRESS*(if different from Controlling Office)*		15. SECURITY CLASS. *(of this report)* Unclassified 15a. DECLASSIFICATION/DOWNGRADING SCHEDULE

16. DISTRIBUTION STATEMENT *(of this Report)*

Approved for public release; distribution unlimited.

17. DISTRIBUTION STATEMENT *(of the abstract entered in Block 20, if different from Report)*

18. SUPPLEMENTARY NOTES

19 KEY WORDS *(Continue on reverse side if necessary and identify by block number)*

Ceramic materials	Silicon nitride
Life expectancy	Glass ceramics
Disks	Gas turbine
Test and evaluation	Brittle materials design

20. ABSTRACT *(Continue on reverse side if necessary and identify by block number)*

DD FORM 1 JAN 73 1473 EDITION OF 1 NOV 65 IS OBSOLETE

UNCLASSIFIED

SECURITY CLASSIFICATION OF THIS PAGE *(When Data Entered)*

Block No. 20

ABSTRACT

Fast fracture and stress rupture data were collected on two materials, a sintered silicon nitride and a lithium-aluminum-silicate. The fast fracture data was presented graphically in the form of Weibull plots of percent failed versus failure stress. The stress rupture results were presented in tabular form. Photo-micrographs were presented to illustrate the fracture surfaces of fast fracture and stress rupture failures.

A program of specimen development was conducted. The objective of the program was to develop processing techniques to make it possible to fabricate integral shaft spin disks suitable for hot spin testing as stress rupture specimens. The hot spin disk stress rupture results were to be used to correlate experimental time dependent failure results with analytical time dependent failure results.

In the specimen development program several sets of experiments were conducted. The molding experiments determined the relationship of molding conditions to quality after molding, and the relationship of molding conditions to quality after binder removal. The binder removal experiment examined the relationships between pressure and heating rate on the quality of the part. The strength experiment examined the relationship between strength, microstructure, and sintering conditions.

Also as part of the specimen development program the cooling pattern of the green injection molded integral shaft spin disk was studied using finite element techniques. This study was conducted in order to determine a cooling method that left no isolated thermal hot zone in the disk. Experience had shown that such a zone caused a void due to shrinkage. The results of the study were presented as temperature contour plots of the disk and die versus time.

A program of attachment development was conducted. The integral shaft spin disk required a new attachment design. It is a boreless design; therefore, the tie bolt and Curvic Couplings™ used in previous hot spin testing could not be used. Attachment designs utilizing high expansion plastics to accomodate the difference in thermal expansion between ceramics and metals were developed in bench rigs and the hot spin rig.

FORWARD

This report presents the work completed during the period of January 1, 1983, through December 31, 1985, on the "Methodology for Ceramic Life Prediction Program," initiated by Mr. Robert Schulz of the Office of Conservation, Division of Transportation systems, Department of Energy, and monitored by the Army's Materials Technology Laboratory under Contract Number DAAG-46-77-C-0028. Funds for this phase of the work were provided by the Department of Energy. This work was necessary in formulating a methodology for ceramic life prediction so that ceramic materials can be used in high temperature structural applications. The principal investigator of this program was R. R. Baker, Ceramic Materials Department, Research Staff, Ford Motor Company. The technical monitor was Dr. E. M. Lenoe of MTL. The authors wish to thank Drs. E. M. Lenoe, R. N. Katz, and Mr. G. D. Quinn of MTL for suggestions in carrying out the program.

TABLE OF CONTENTS

I. INTRODUCTION

The objective of this program was to establish a methodology for predicting the lifetime reliability of structural ceramic materials in high temperature applications. The program consisted of two interrelated parts: one the determination of statistical and time-dependent strength characteristics of selected structural ceramic materials as a basis for analytical life prediction; two, the design and hot testing of ceramic components which are exposed to high enough temperatures to have time dependent reliability. The data gathered in part one was used to predict the time dependent reliability of the components in part two. The experimental time dependent reliabilities determined by the testing required in part two were compared to the predicted time dependent reliabilities to verify the analytical models.

As the program evolved additional tasks were undertaken in order to support the original program objectives. The design, test, and evaluation of ceramic to metal joints was undertaken in order to support the program requirement for a reliable attachment method for integral shaft spin disk. Also a specimen development task was undertaken in order to meet the requirement for an integral shaft spin disk with properties suitable for hot testing with time-dependent failure conditions prevailing.

Early work in the program was concentrated on gathering time dependent properties of two materials; Norton's NC-132 and Ford's hot pressed silicon nitride (HPSN) containing 3.5% MgO. The principal time dependent property measured was the crack velocity exponent. This was done by three methods; double torsion testing, stress rate testing, and flexural stress rupture testing. Also fast fracture testing with precracked specimens was used to determine inherent flaw size. Flexural stress rupture testing was used to determine the time to failure of the materials under constant stress and temperature conditions. This early work together with a procedure for measuring fracture mechanics parameters was documented by Govila[1,2,3,4].

The next phase of the program concentrated on developing and utilizing tensile testing to gather time dependent material parameters. Fourteen tensile stress rupture tests were conducted at 1000°C, sixteen tests at 1200°C, and eleven tests at 1300°C. In addition some precracked tensile stress rupture specimens were tested. The crack velocity exponent was determined at 1200°C from the tensile stress rupture tests. The material

used for these tests was NC-132. In addition the crack velocity exponent and pre-multiplier at 1300°C, 1350°C, and 1400°C were determined for NC-132 using double torsion methods. As a follow on to previous work, additional flexural stress rate and stress rupture testing was conducted on NC-132 and Ford's 3.5% MgO HPSN. This work was documented by Govila[2,3,4,5].

Silicon carbide was added to the program early in 1980. Carborundum's sintered alpha silicon carbide was selected for extensive testing. Fast fracture testing was conducted to determine the materials strength versus temperature. Eight tensile stress rupture tests were conducted at 1200°C and seven tests at 1300°C. The crack velocity exponents were determined from these tests. Flexural stress rupture tests were conducted at 1300°C and 1400°C. The crack velocity exponents were determined at 1300°C and 1400°C from these tests. Extensive fractography was conducted on the failed specimens to document the causes of failure, flaw size, and flaw location. This work was published by Govila[6,7,8].

As part of the program's continuing investigation of analytical and experimental methods in ceramic life prediction aimed toward utilizing structural ceramics in practical applications, a component was selected for analysis. The component selected was the hub of a hot pressed silicon nitride turbine rotor. The required geometrical, material, strength, and time dependent data was supplied by MTL. A finite element computer model was prepared for the disk from this data. The temperature and stress distributions, the fast fracture and the time dependent reliabilities were calculated. The results were presented in isostress and isothermal plots for the combined centrifugal and thermal loadings as well as isostress plots for the centrifugal loadings. The reliability versus time for the disk to 1000 hours was calculated and presented graphically. The work was documented in a technical report by Swank[9].

The data generated in the early phases of the program was used to design a NC-132 bladeless turbine disk which was tested in a hot spin test rig. The disk was designed to fail due to time dependent mechanisms. Several disks were fabricated and an existing test rig was developed to test the disks. Ten disks were tested at steady state under the design conditions of 2300°F rim temperature and 50,000 rpm for periods of 0.20 hours to 25 hours. Six disks failed due to time dependent failure and four tests were suspended. An experimental failure distribution was obtained for the ten disks and presented as reliability versus time. Three different data bases (double torsion, stress rate, and stress rupture) were used to calculate reliability versus time and results were compared to the experimental results. The best correlation with experimental results was with stress rupture data. The results of this effort were documented by Baker et al[10,11].

The results of the NC-132 bladeless disk testing suggested repeating the tests with another material to confirm the conclusion that the stress rupture data base was the best data base to use for calculating reliability versus time. Accordingly a proposal was made to conduct a similar series of tests utilizing an integral shaft spin disk. This disk would simplify the mechanical mounting if an appropriate attachment system could be developed. The integral shaft disk attachment would be more reliable than the tie bolt and face spline attachment used with the NC-132 disk. In addition, it offered the possibility of being able to start-up and shut-down the test several times, something not possible with a face spline attachment. This would mean that tests could be conducted for longer periods of time eliminating suspensions, and giving a better experimental failure distribution.

This report covers the last segment of the program, where the effort was directed toward repeating the bladeless disk testing. Initially the program planned on using existing materials for disk fabrication. These materials required extensive flexural fast fracture and stress rupture characterization to build the data base required to design the disk and select the test conditions. As the existing materials were characterized it became apparent that their development was not at a state were a successful correlation program could be executed. At that point the program was modified to include a period of specimen development to bring the materials up to a point where a successful disk program could be conducted. Along with this work an attachment development program was conducted in order to develop and verify a metal to ceramic attachment suitable for conducting long term tests of an integral shaft spin disk.

II. DATABASE COLLECTION

A. Silicon nitride data

For the characterization of a silicon nitride material Ford supplied billet A-42 of RM-20, a sintered silicon nitride. This material contained 8 weight percent yttria as the major sintering additive. This material was found to be suitable for slip casting gas turbine engine components such as rotors and adiabatic diesel engine parts. Sintering was done in a nitrogen environment without any over pressure. For this study, the material was cold pressed, nitrided and sintered in the form of a rectangular billet.

Flexural test specimens 1.25 inches long by 0.25 inches wide by 0.125 inches thick were machined from billet A-42. All faces were ground lengthwise using 320 grit diamond wheels, and the

edges were chamfered lengthwise to prevent edge effects. For flexural strength evaluation, specimens were tested in four-point bending in an Instron testing machine, Model 1125, using a specially designed self-aligning ceramic fixture made from hot-pressed SiC[2]. The inner and outer knife edges of the testing fixture were spaced 9.5mm and 19mm apart, respectively.

The flexural stress rupture tests at elevated temperatures (800°C to 1200°C) in air were conducted in four-point bending using the self-aligning ceramic fixture and a rapid temperature response furnace. The load was applied to the test specimen through a cantilever arm, deadweight assembly. The experimental set-up was equipped with a microswitch to cut off the power to the furnace and the timer at the instant failure of the specimen occurred. The total time to failure was recorded. An overall view of the test set-up and complete details regarding the design and operation of the stress rupture test rig are given elsewhere[12].

At room temperature, ten specimens from billet A-42 were tested in four point bending to determine the fast fracture strength. The statistical variation in fracture strength at room temperature is shown in Fig. 1. The fracture strength varied from a minimum of 785 MPa to a maximum of 988 MPa with an average strength of 873 MPa, standard deviation of 79 MPa and a Weibull modulus of 13.

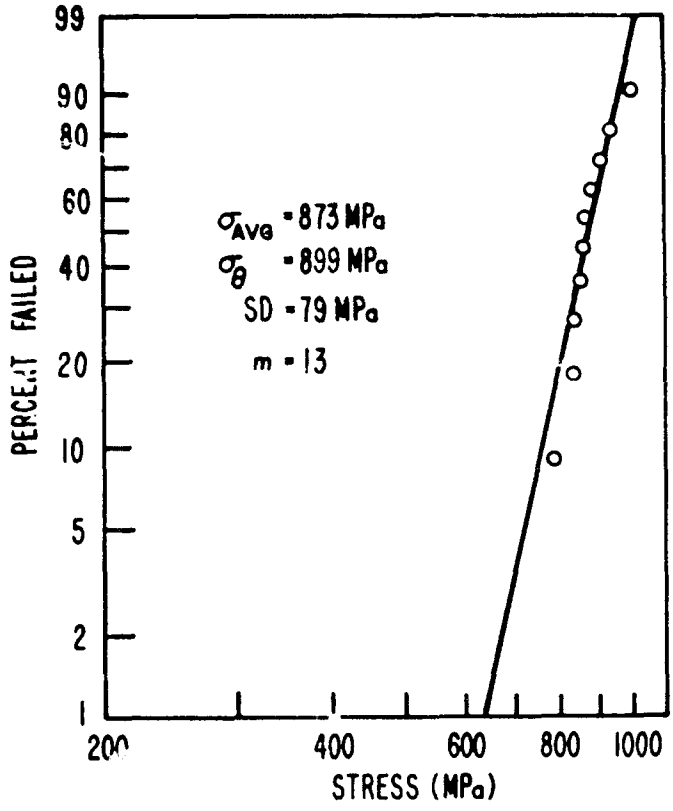

Fig. 1. Weibull probability plot of billet A-42.

Examination of the fracture surfaces revealed that all failures in specimens tested at room temperature were associated with porosity in the material. Typical failure occurring at a porous region is shown in Fig. 2. These porous regions were approximately 50 micrometers wide and 100 micrometers deep as shown in Fig. 2. Closer examination of the flaw site revealed that the grain morphology of beta silicon nitride inside the porous region appeared to be primarily needle shape (accicular) and less accicular away from it, Fig. 2(b).

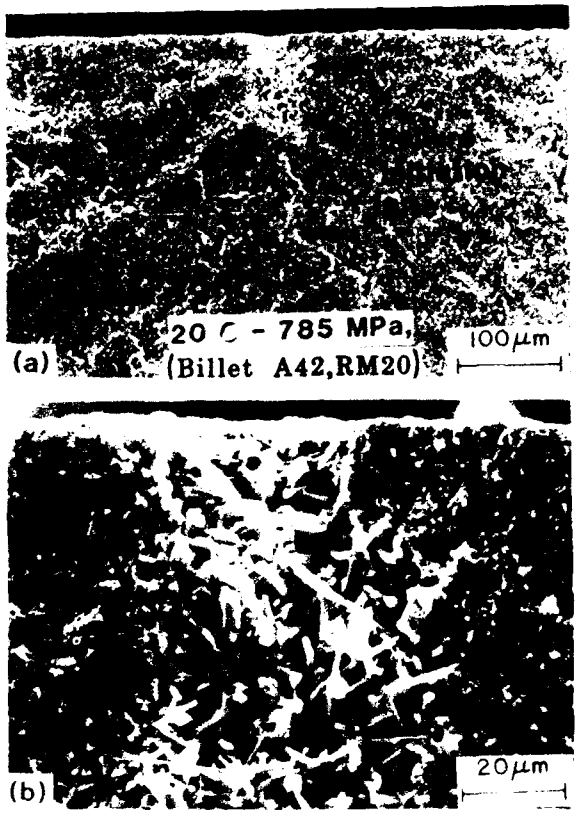

Fig. 2. Typical fast fracture surface.

Stress rupture testing was carried out in order to determine if the RM-20 material was susceptible to instability in the intermediate temperature range from 600°C to 1000°C. A total of six specimens were tested in stress rupture mode and the results are summarized in Table I. At 800°C, one specimen was tested at an applied stress level of 413 MPa and sustained the stress for over 300 hours without showing any signs of bending or failure. A second specimen tested at 482 MPa, failed in 88 hours. The fracture surface showed a porosity associated oxidized region, Fig. 3. Away from the fracture origin, the fracture surface showed the smooth appearance of crack propagation indicating trans-granular fracture, Fig. 3(C).

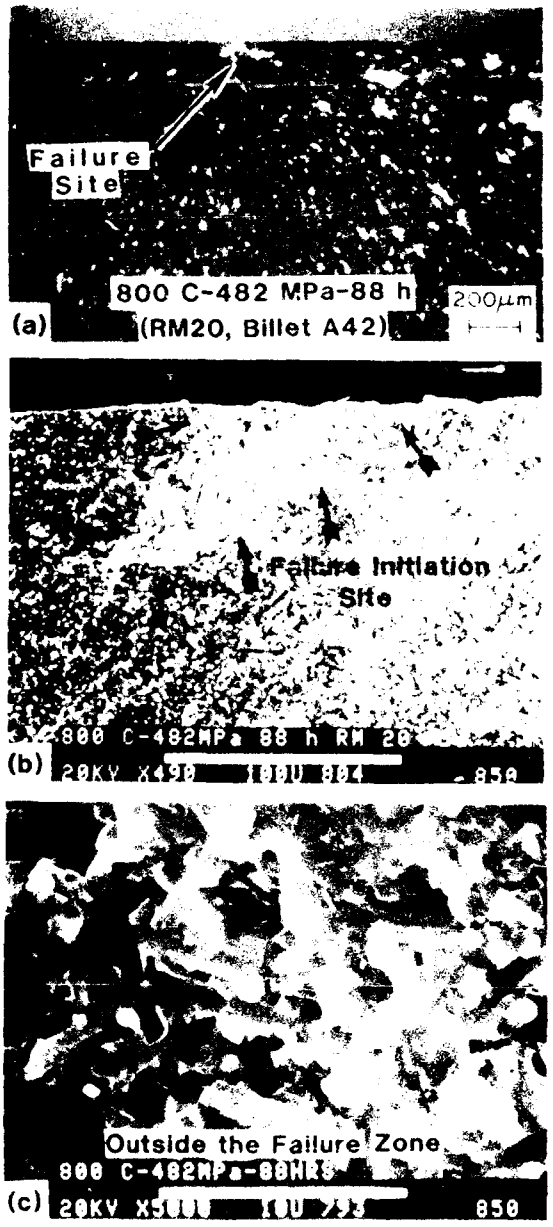

Fig. 3. Stress rupture fracture surface.

At 1000°C, the material showed a distinctly different behavior than that seen at 800°C. Two specimens were tested at the low stress level of 344 MPa. One survived 306 hours without failure or bending while the second specimen failed in 35 hours. Examination of the fracture surface revealed the presence of a

locally oxidized region as the failure initiation source. A third specimen was tested at 413 MPa. The time to failure decreased significantly with failure occurring in one hour. Examination of the fracture surface revealed failure occurring at a porosity associated oxidation pit, Fig. 4. A fourth specimen, tested at 482 MPa, failed in one-half hour. In brief, this short study showed that Billet A-42 material has oxidation instability at 1000°C. It should be pointed out that in this material, all failures were associated with porosity and this problem can be overcome by proper sintering conditions. Current work at Ford Motor Company is being directed to improve this material.

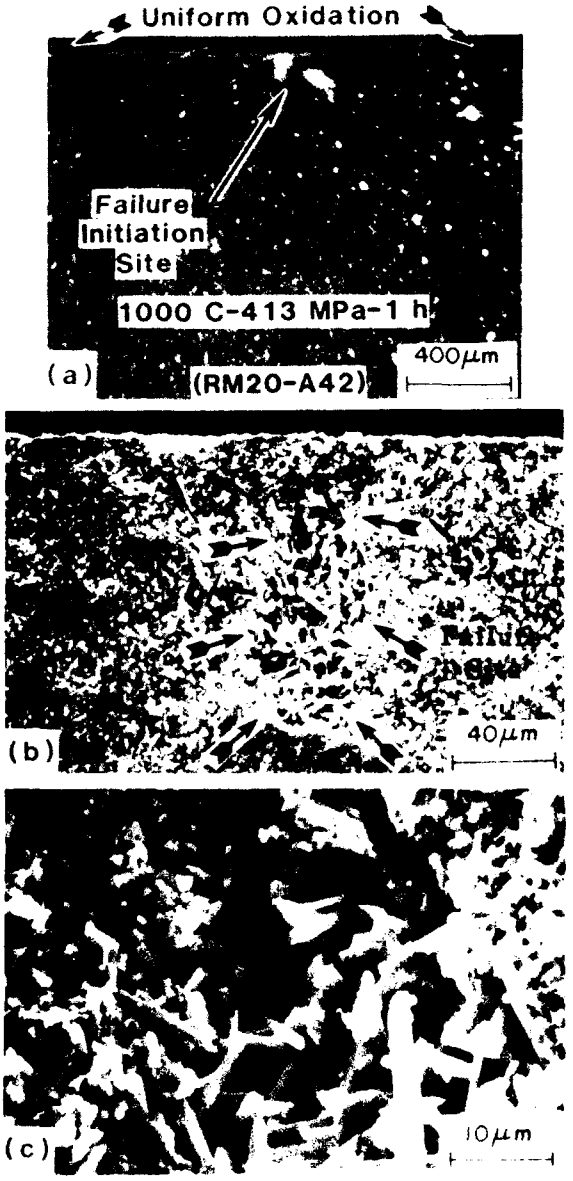

Fig. 4. Stress rupture fracture surface, 1000C.

B. LAS Data

For the characterization of LAS material Ford supplied LAS plate serial number A18C-7. The plate was machined into .125in x .25 in x 1.25 in bars and 1.00in x 1.00in x .696in blocks. All test bars were X-rayed to insure that they were free from internal flaws. Fast fracture testing was conducted on thirty bars to establish the baseline strength. The Instron machine head speed was 0.5 mm/minute. The characteristic modulus of rupture was 139 MPa with a Weibull modulus of 10.0. The distribution mean was 133 MPa and the standard deviation was 16.0 MPa. The sample range was from 99 to 160 MPa. Examination of the fracture surfaces revealed that the majority of the failures were surface originated. The statistical variation in fracture strength is shown in Fig. 5. Complete strength data for the fast fracture tests is given in Table II.

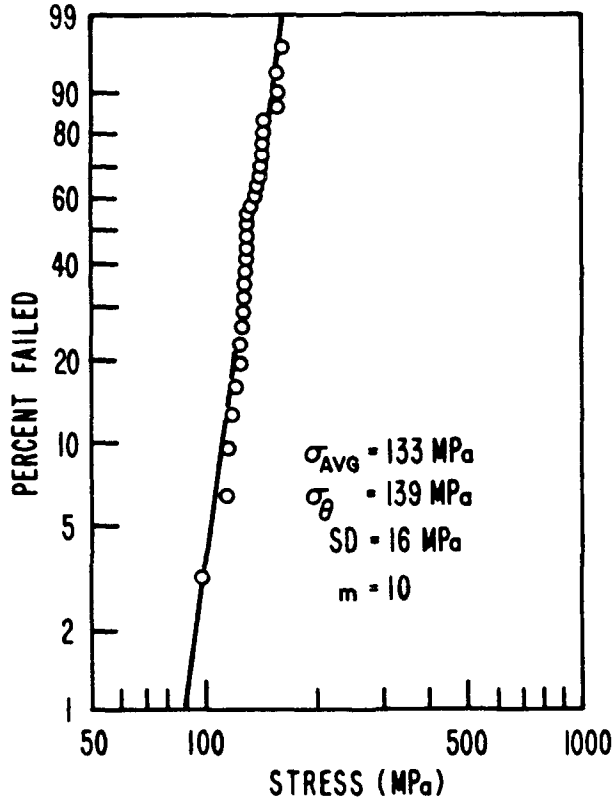

Fig. 5. Weibull probability plot of LAS.

Ten LAS specimens were prepared for flawed beam stress rupture testing by precracking using a Vickers diamond pyramid indenter with a 1000 gram load. This controlled precracking method introduces an approximately semi-circular crack of 48 to 55 micrometers deep. Table III summarizes the flawed beam

results which are discussed in detail in the following paragraphs.

Two precracked specimens, numbers 31 and 32 in Table III, were tested at room temperature in four-point bending in order to determine the materials strength and to show the nature of the crack front geometry (semi-circular, ellipsoidal, or other form). The specimens failed at 93 and 114 MPa, respectively. Typical crack front geometry showing the semicircular crack front due to precracking with 1000 gram indentation load is shown in Fig. 6, which illustrates the fracture face of specimen 31.

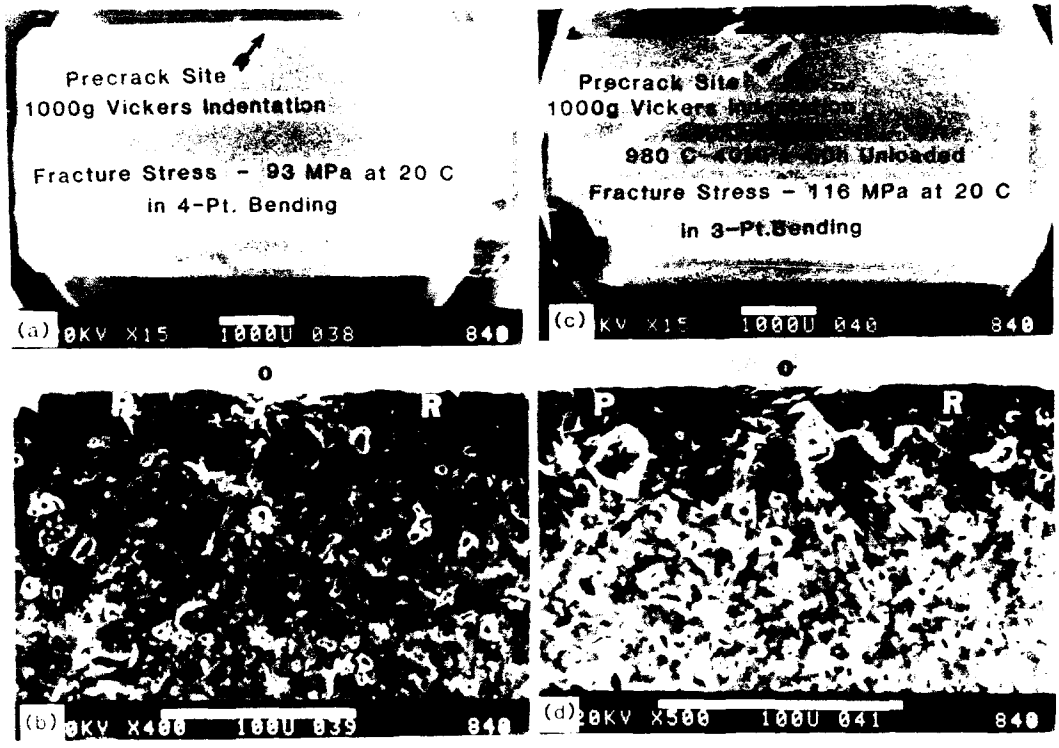

Fig. 6. SEM fractographs of LAS specimens.
(a) View of fracture surface, pre-cracked specimen tested at room temperature.
(b) Higher magnification view, PQR is approximately the crack front boundary.
(c) View of fracture surface, pre-cracked stress rupture specimen. Specimen was unloaded and fractured at room temperature.
(d) Higher magnification view of the pre-cracked region PQR seen in (c). Note, the fracture surface is smooth and similar to that seen in (b).

Two precracked specimens were tested in stress rupture at 871°C under applied stress of 40 MPa, without failure for 93 and 50 hour, respectively. After the stress rupture testing was

completed both specimens were tested in 3-point bending using a machine head speed of 0.5 mm/minute at room temperature in order to reveal if any subcritical crack growth occurred. Neither specimen failed at the precrack site, but failed away from it suggesting crack blunting or healing. Similar behavior was noted for the two specimens, numbers 35 and 36 in Table III, tested at the same applied stress of 40 MPa, but at a temperature of 927°C. Both sustained 50 hour without failure.

Four precracked specimens were tested at 982°C and at an applied stress of 40 MPa. All sustained 50 hour without failure. These specimens were then tested in 3-point bending at room temperature and only one failed at the precrack site (specimen 37, Table III) and the remainder failed away from the precrack site suggesting crack blunting or healing. The fracture surface for the specimen 37, which failed at the precrack site, is shown in Fig. 6. The semi-circular crack front region PQR is visible and shows smooth re-propagation of the crack. No signs of any subcritical crack growth were seen in this specimen. This behavior is similar to that seen in a fully dense LAS in an earlier study, Govila et. al.[13]. Therefore, it is concluded that this LAS does not undergo creep deformation at 982°C under an applied stress of 40 MPa as indicated by flexural stress rupture tests. It is quite possible that the material may undergo creep deformation if the applied stress is increased.

Application of LAS as a structural ceramic material generally requires long term thermal stability. To evaluate the thermal stability of the Ford LAS, sixteen blocks were precision ground from the A18C-7 plate. The blocks were divided into four groups. Five for thermal stability testing at 1600°F, five for testing at 1700°F, five for testing at 1800°F, and one block to serve as a control. The blocks were measured in a temperature controlled room, with the temperature held at 68°F, plus or minus 0.5°F. The pattern of measurements is shown in Fig. 7. The xyz axis was identified on each block by a small chamfer on the 0-0-0 corner. Along the x and y axis the blocks were measured in five places, and along the z-axis the blocks were measured in the center. The reason for the limited measurement in the z-direction was that the surface normal to the z-axis was used to rest the block on when it was in the oven; therefore, it was considered inappropriate to consider the z-direction as critical to the experimental results.

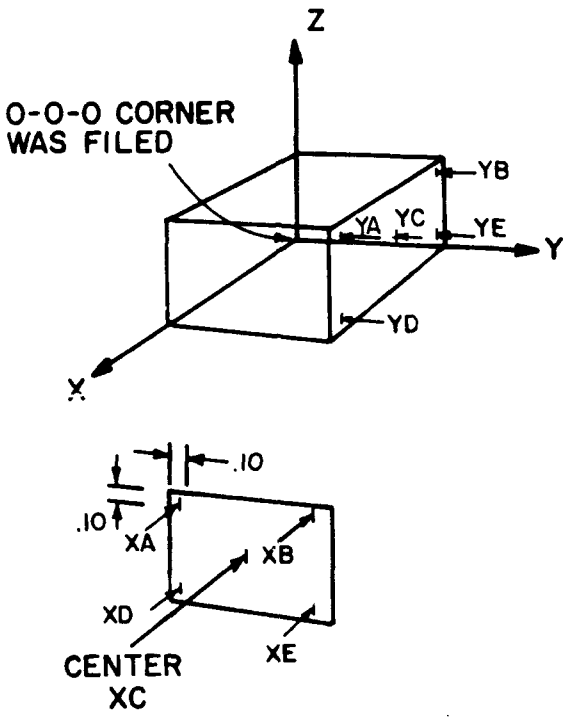

Fig. 7. Thermal stability block measurement pattern.

Electric ovens were used to conduct the thermal stability tests. Samples were removed from the ovens at 285, 500, and 1000 hours for measurement. The results are shown in Table IV. In addition to dimensional measurements the blocks were weighed to four decimal places in grams and the results are shown in the table. The sample range was determined for each dimension and is shown on the table.

Review of the data and comparing the results of the blocks thermally soaked versus that of the control block, indicate that the LAS was thermally stable over the temperatures and times tested.

III. SPECIMEN DEVELOPMENT

A. Introduction

The objective of the specimen development part of the program was to develop the methodology to fabricate the Integral Shaft Spin Disk (ISSD), Fig. 8., using an injection molded, sintered reaction bonded silicon nitride (IM-SRBSN). The ISSD's were to be used in a series of stress rupture tests conducted in the hot spin rig to provide additional data for the verification of time dependent failure theories.

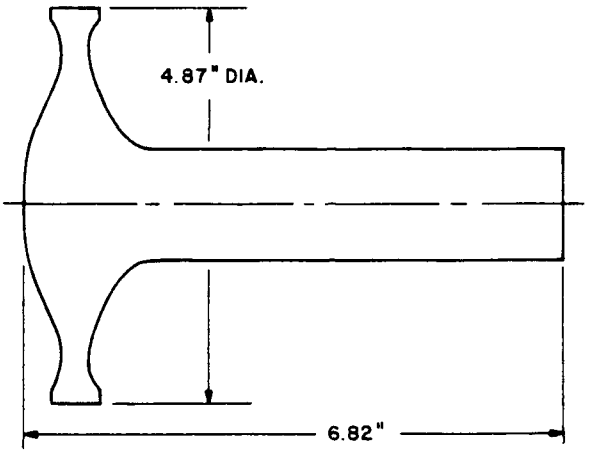

Fig. 8. The integral shaft spin disk (ISSD).

Ford has had considerable success with the injection molding process for both thin and thick cross-section components as shown in Figures 9, 10, and 11. Relative to thick cross-section components, Ford has demonstrated that turbocharger and AGT rotors can be molded without internal voids or external cracks. Respectable processing yields have been obtained for turbocharger rotors. It has also been demonstrated that these thick cross-section components can be processed through the binder removal process without the creation of additional voids, although the processing yields are much lower.

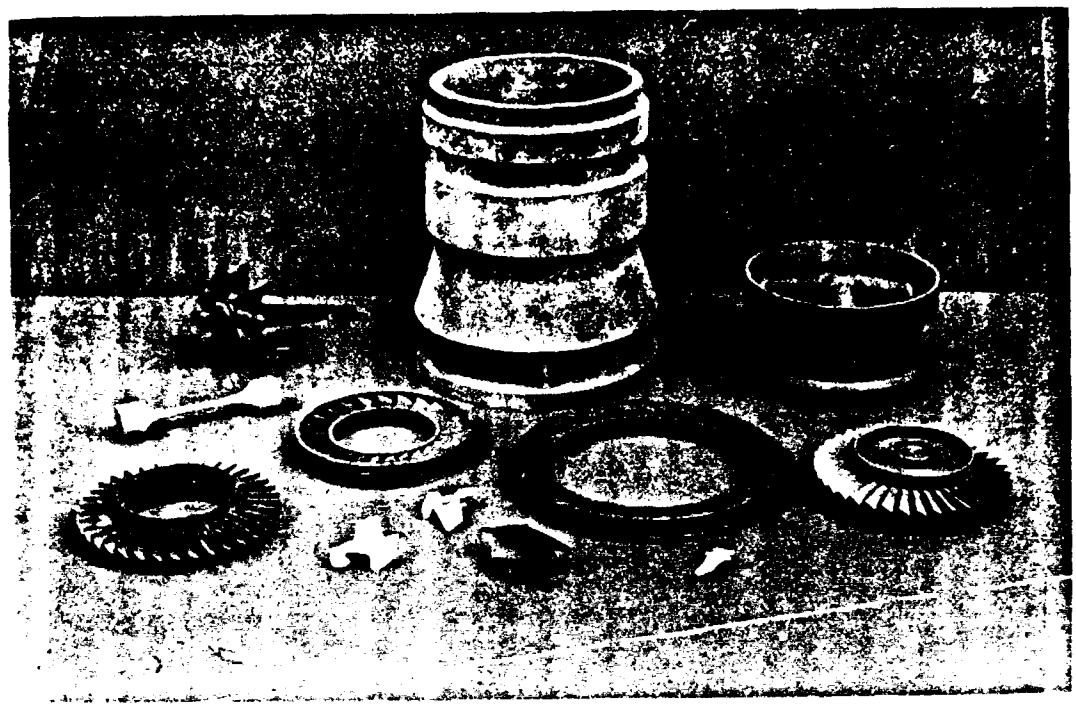

Fig. 9. Ford injection molded components having thin cross-sections.

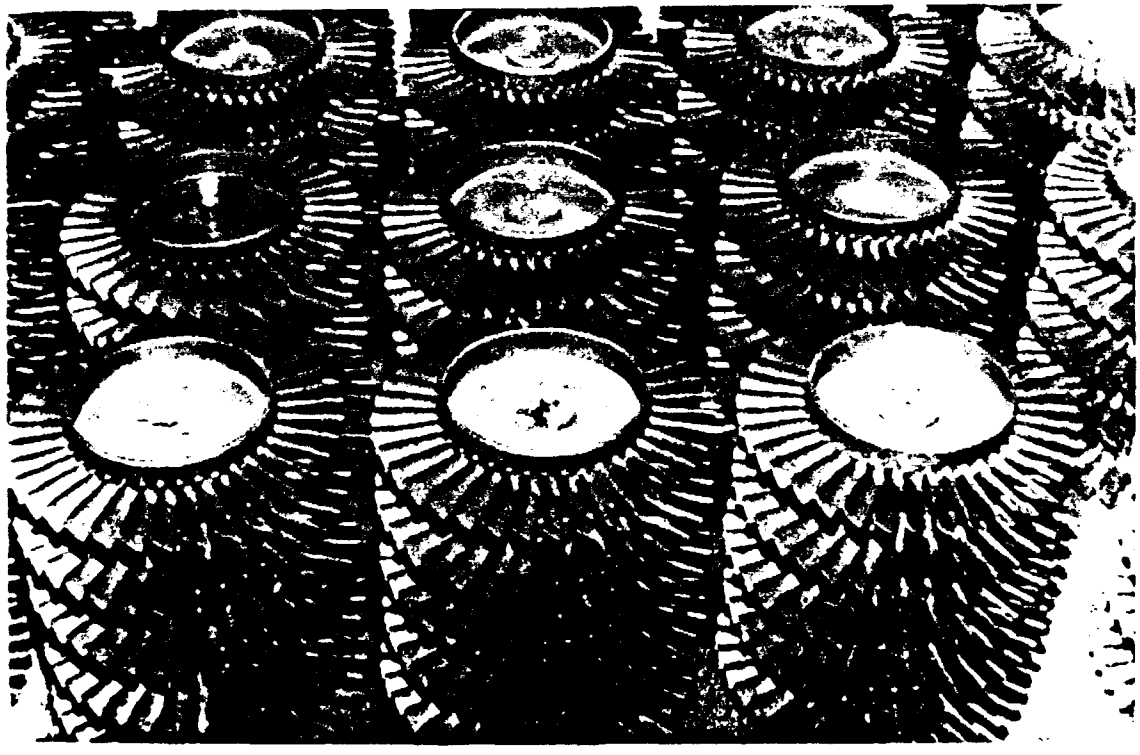

Fig. 10. Ford high volume injection molding components.

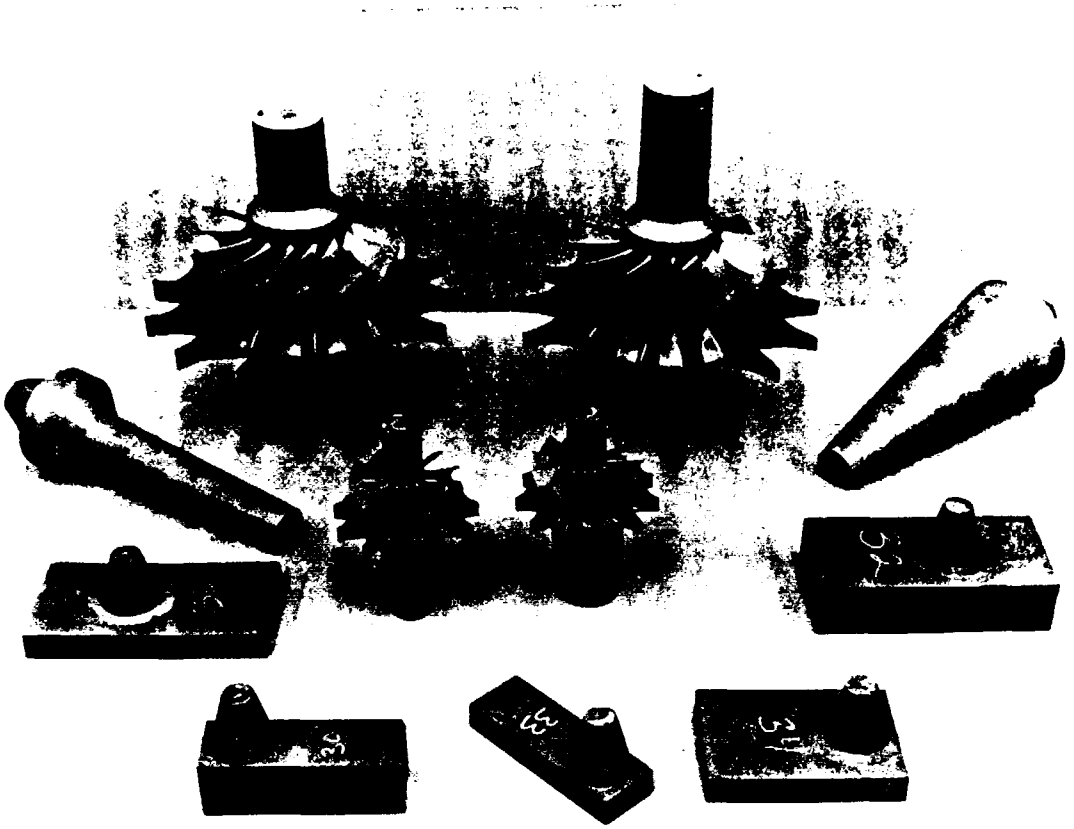

Fig. 11. Ford injection molded components having thick cross-sections.

Ford has also had considerable success in the development of sinterable silicon nitrides of which SRBSN is one type. During the course of these developments, Ford has gained experience in nitriding and sintering technology as well as in material characterization of both fast fracture and time dependent properties. Ford has also developed the technological expertise to tailor a material to a particular property requirement.

The individual processing steps required for the successful fabrication of an ISSD have been demonstrated. However, further development work was required to improve the process consistency, improve the overall process yields at each process step, and to further improve the properties of the IM-SRBSN material. The major development step was the scaling of the process to accommodate the larger ISSD geometry.

The specimen development work was divided into two major areas: (1) injection molding, and (2) sintering-property development. Fig. 12. illustrates the specific processing steps included in each area. The experimental program focused research on the known problems, which were identified prior the initiation of the contract, and were known to affect the fabrication of a large, thick cross-section component such as the ISSD.

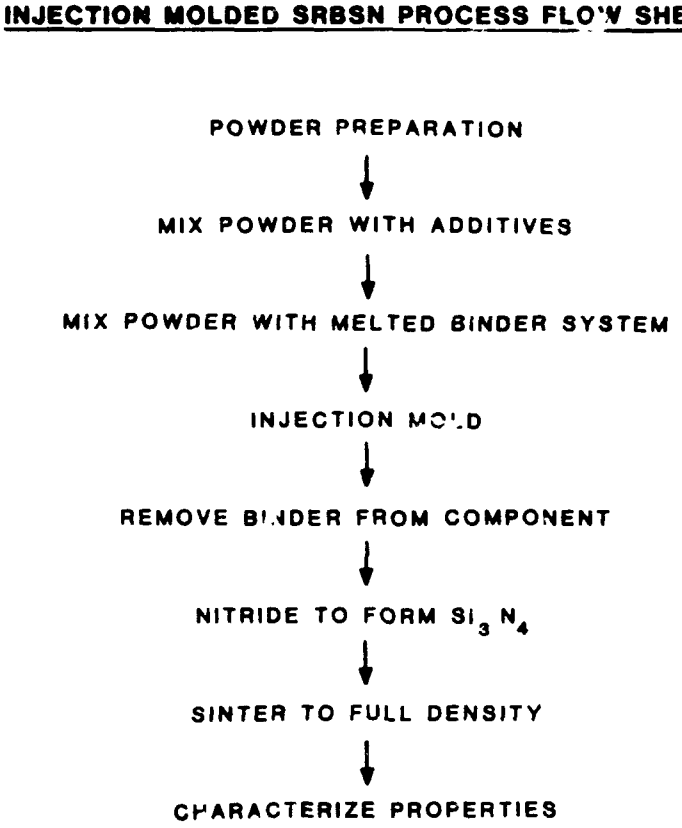

Fig. 12. Injection molding process flow sheet.

The following sections will describe the results of processing experiments designed to attack specific problems. Since the program was terminated prior to the completion of the planned program, these individual experiments stand alone. The tasks which would have brought the experiments together, resulting in the successful fabrication of an ISSD, were not funded.

B. Injection molding experiment

A set of statistically designed experiments was performed to relate the effect of four injection molding variables to component quality after molding and after binder removal. It was shown that the magnitude of these variables directly effect the quality of the components after binder removal. The results are

consistent with a general, qualitative model relating the quality of the component to the stress state developed in the component during molding.

It has been demonstrated that a number of components of differing geometries can be injection molded. Visual inspections after molding show that all of these components can be molded without visual defects (such as cracks); however, the molding yield may vary with the particular geometry. It has also been demonstrated that in general these components will develop cracks during the binder removal process. The severity of these cracks appear to be a function of the component's geometry. The cracks generally occur in locations having severe section changes. These locations would be expected to be "high" stress areas.

Many discussions have centered on the question of the presence of residual stresses within the molded article and whether the stress state of the molded article causes cracking during binder removal. It is generally agreed that changes in molding conditions should affect the stress state of the part; however, no experimental technique has been identified which can measure the residual stresses in a molded ceramic article. The purpose of the injection molding experiment was to determine if changes in molding conditions result in changes in the observed cracking after binder removal.

This experiment evaluated the effect of four injection molding variables on part quality after molding and after binder removal. The injection molding variables were die temperature, injection pressure, material temperature, and hold time. A 2^{4-1} fractional factorial experimental design[14], shown in Table V, was employed. The experiment was repeated for two components, each representing some feature of the ISSD. A number of responses were measured and are summarized in Table VI.

Two responses are considered critical after molding: (1)density, and (2)the number of x-ray indications. The quality parameters relating to cracks are only important after binder removal. Table VI summarizes the direction each variable must be changed from the average value to effect an improvement in the component quality after molding.

The responses of importance after binder removal are those related to cracking. Three types of cracks were common for the components molded in this study. While responses of these type of defects were analyzed after molding, it was determined that these responses after binder removal were the ones which were critical to the production of quality components. Data was obtained after the binder removal process. Table VII shows the direction each variable must be changed from the average value

in order to improve component quality, that is minimize each type of crack.

The nature of the experimental design resulted in the determination of the effect of the four variables on the various responses. However, because this was a fractional factorial experimental design, the interaction between variables could not be determined. This design was used as a screening experiment to identify the variables having a major effect on the responses and to identify the direction in which to change these variables in future experiments.

The results generally indicate that all four injection molding variables, die temperature, injection pressure, material temperature, and hold time should be reduced in order to improve the component quality. The results all generally appear to be consistent with a shrinkage/stress model. They show that conditions which are thought to a yield low stress state in the component also result in a high quality component after molding and binder removal. They also show that the molding conditions directly effect the quality of the component after binder removal.

C. Binder removal experiment

A set of statistically designed experiments was performed to determine the effect of three binder removal processing variables on the component quality after binder removal. The results indicate that complex components can be successfully processed through binder removal over 10 times faster with the use of a pressurized binder removal atmosphere. The results also show simple components can be successfully processed at these high rates without the necessity of the pressurized atmosphere.

Binder removal is the most difficult processing step in the injection molding process, and it has probably been the least studied. A large number of processing variables exist which could effect the quality after binder removal. This experiment studied three of those variables.

A set of experiments were designed to determine the effect of three processing variables on the component quality after binder removal. The variables investigated were: (1) the pressure of the binder removal atmosphere, (2) the rate of temperature rise, and (3) the complexity of the geometry of the component. A full factorial 2^3 experimental design, shown in Table VIII was employed to determine primary effects as well as interaction effects.

The analysis of the binder removal results is presented in Table IX. The results indicate that higher binder removal percentages are obtained at high pressure than under low pressure conditions. This was found to be true for both the large and small component. The results also indicated that the large complex component exhibits higher binder removal percentages than the small component. This result is surprising and may be due to the fact that different materials were involved in the fabrication of the large and small components.

The results were re-analyzed using only the large component. These are summarized in Table X. These results indicate that the maximum binder removal occurs at high pressure and low heating rate. An interaction between these two variables is present, as illustrated in Fig. 13.

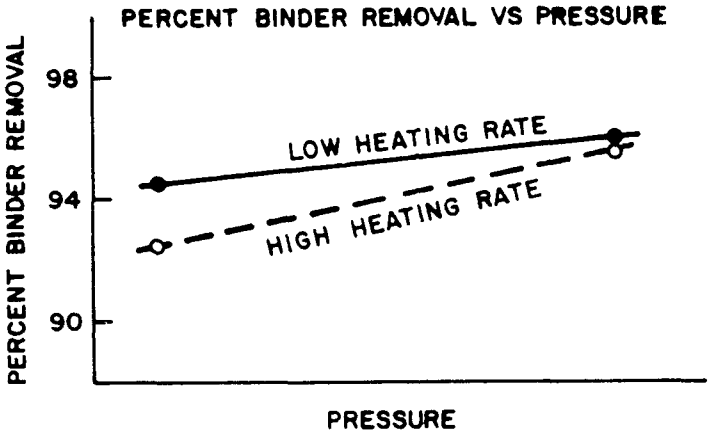

Fig. 13. Percent binder removal versus pressure.

The quality of the components are determined by the number of cracks observed by visual inspection. The results for the complete matrix are presented in Table XI in terms of total cracks. The results indicate that in order to minimize component cracking the pressure should be at the high level. These results also show that small, simple components are less susceptible to cracking than large, complex components. There is a strong pressure-size interaction which is illustrated in Fig. 14.

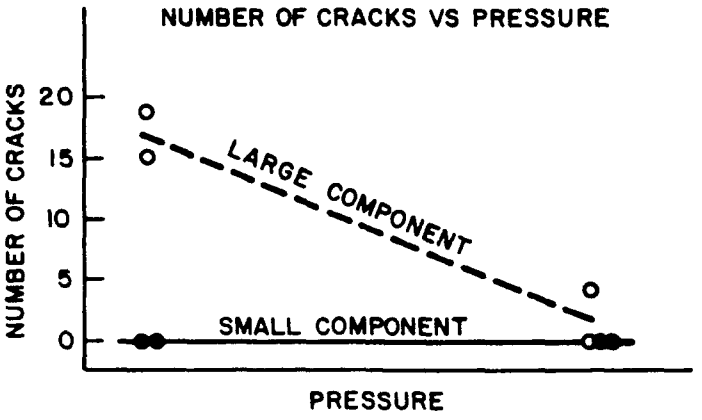

Fig. 14. Interaction of pressure and component size on the number of cracks after binder removal.

The cracking results were re-analyzed for the large component only. These results are summarized in Table XII. All results show that the amount of cracking in large components can be minimized by performing the binder removal at high pressure. Pressure-heating rate interactions are also present, as illustrated in Fig. 15.

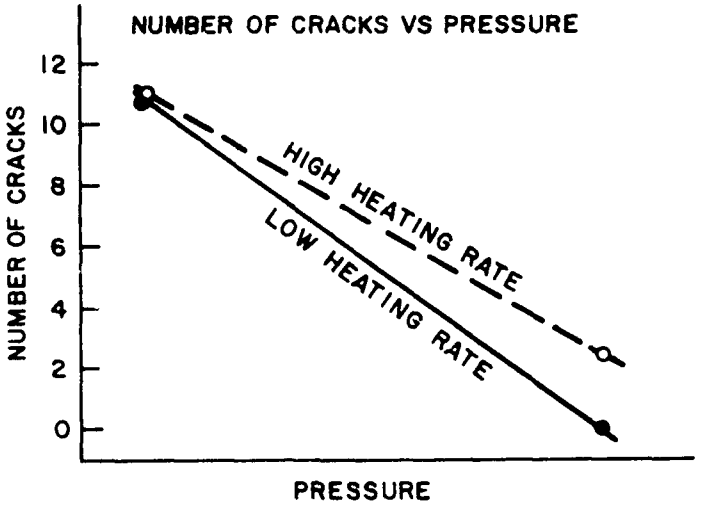

Fig. 15. Interaction of pressure and heating rate on the number of cracks after binder removal.

Binder removal using increased pressures result in improved quality components. The binder removal percentages are higher and the amount of cracking is reduced. Additionally, the binder

removal times can significantly be reduced. For large components, binder removal times were reduced by a factor of six with no reduction in quality, as measured by percent binder removal or number of cracks. The mechanism for the beneficial effect of pressure is unknown.

D. Microstructure development

The analysis of the microstructures of a number of compositions within the yttria/alumina system showed that a critical temperature exists above which exaggerated grain growth occurs and below which a uniform microstructure can be obtained. Sintering time above the critical temperature was identified as the principal parameter contributing to excessive grain growth.

Prior to the receipt of this contract, a number of compositions in the yttria/alumina system were dry pressed, sintered and characterized. The purpose of this study was to determine the processing parameters responsible for the development of the unique microstructural features responsible for the failure origins within these materials. Attempts were made to quantify the microstructure obtained by SEM analysis. The maximum grain size and the number of grains exceeding a particular size were determined.

The microstructure of the yttria/alumina SRBSN materials was determined to consist of a bi-modal type distribution of needle shaped grains having length to diameter ratios of about 5/1 to 10/1. A typical micrograph is shown in Fig. 16. The strength of materials having this type of structure is in the 80-95 Ksi region. A plot of strength versus porosity ,Fig. 17, shows that the strength is independent of porosity. That means another type of defect is the strength controlling parameter. This was determined to be the large, needle shaped grains.

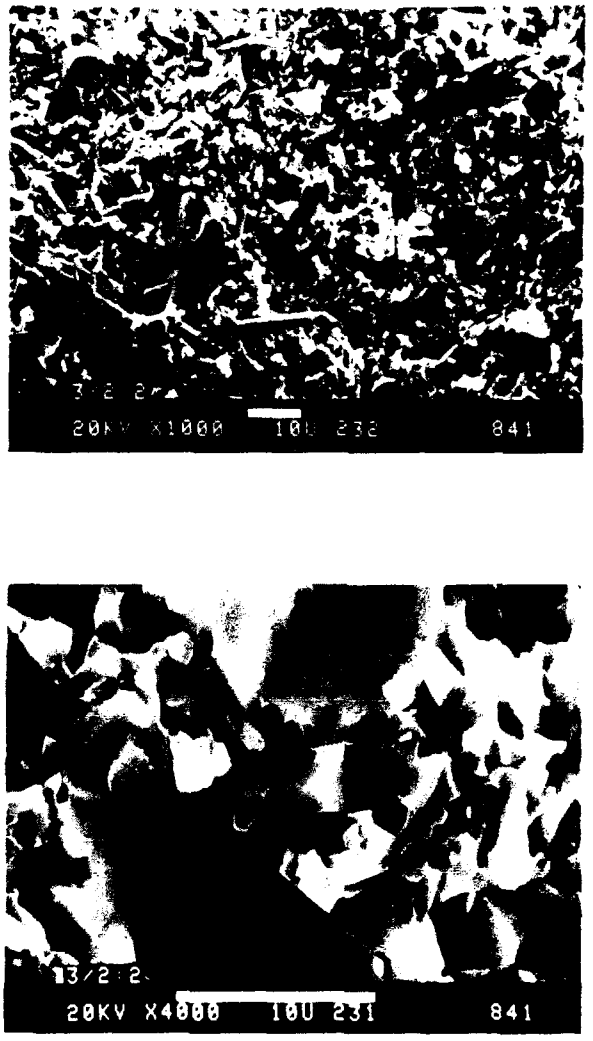

Fig. 16. Typical microstructure of the baseline SRBSN material processed above the critical temperature. The low magnification photo illustrates the exaggerated grain growth, while the high magnification photo illustrates the grain growth of the overall structure.

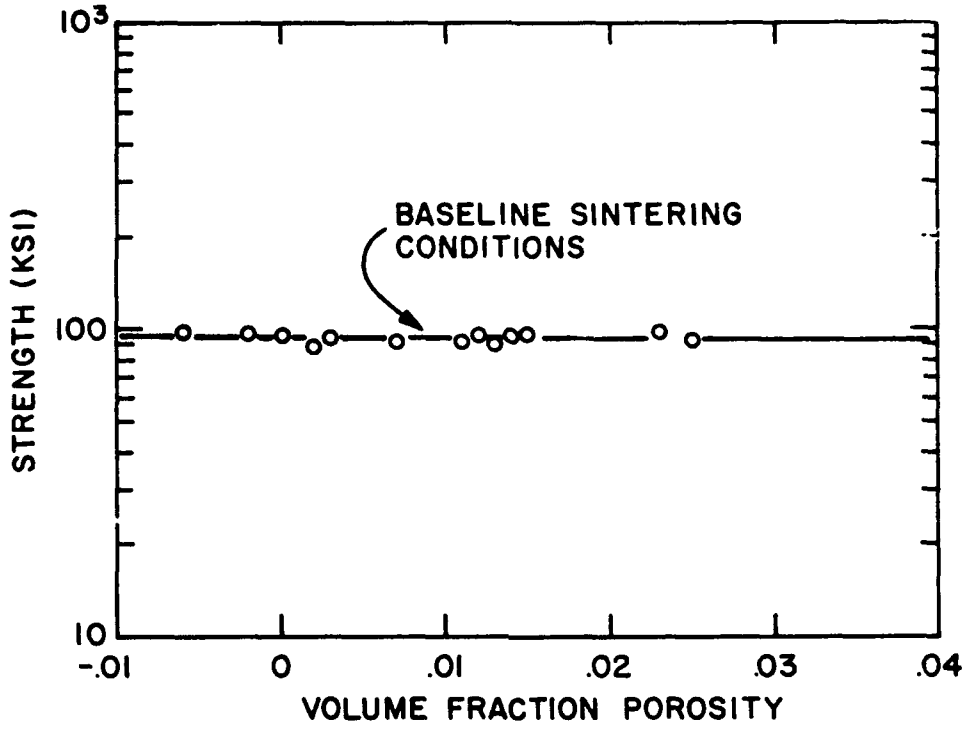

Fig. 17. Strength versus porosity for the baseline SRBSN material processed above the critical temperature.

Examination of the structure of a number of compositions processed using a number of sintering conditions indicate that grain growth occurs above a particular, critical temperature. The data for maximum grain size and the number of large grains per unit area, Figures 18, and 19 both illustrate this finding; furthermore, these figures show that time at temperature above the critical temperature is the significant parameter affecting grain growth.

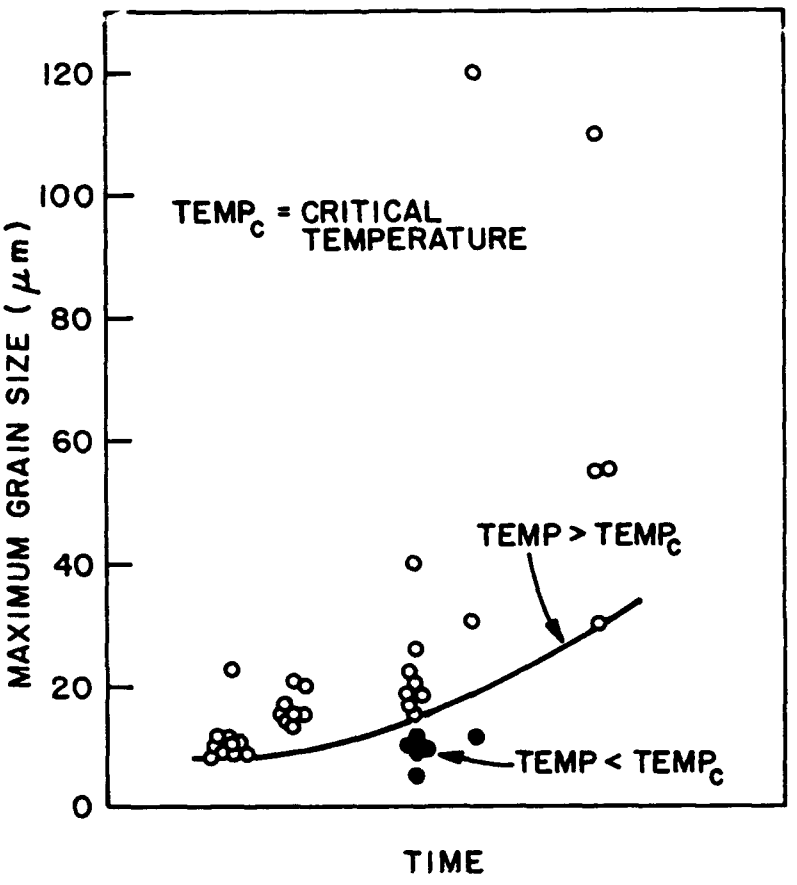

Fig. 18. Maximum grain size versus time. Open symbols indicate samples processed above the critical temperature ($Temp_c$); the solid symbols indicate samples processed below the critical temperature.

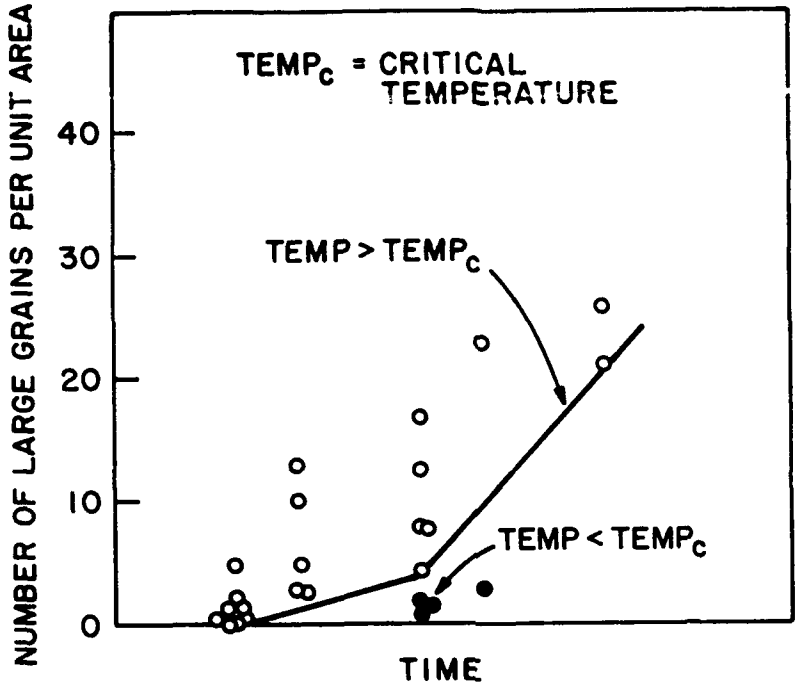

Fig. 19. Number of large grains per unit area versus time. Open symbols indicate samples processed above the critical temperature (Temp$_C$); the solid symbols indicate samples processed below the critical temperature.

These results define a set of acceptable time-temperature sintering parameters required for obtaining a uniform microstructure in a sintered reaction bonded silicon nitride. These results were independent of composition and will serve to guide the processing of new compositions.

E. Strength experiment

Dry pressed SRBSN samples processed using sintering parameters designed to produce a uniform microstructure demonstrated strength improvements of about 35 percent over the baseline established with maximum strengths of 133 Ksi with a Weibull modulus of 22. The strength of injection molded SRBSN, processed using these conditions was 75-88 Ksi. The bulk microstructure of the injection molded material was identical to the dry pressed material, but the failure origins were different. They were identified to be metallic inclusions of silicon and iron.

The strength of SRBSN has been limited by microstructural features, especially large needle shaped grains. The work described in the previous section points out processing techniques which can minimize the exaggerated needle growth in SRBSN materials. This section describes experiments to improve the strength of SRBSN compositions through microstructure optimization.

Dry pressed compositions of SRBSN were sintered using four sets of processing conditions where the sintering temperature and time were varied. They included a baseline where the sintering temperature was above the critical temperature for grain growth and the time was long. The others included short time at high temperature, long time at low temperature (below the critical temperature) and an intermediate time at an intermediate temperature (near the critical temperature). These last three conditions were designed to generate a microstructure free of the large needle shaped grains. The density, strength and microstructure were studied for the four processing conditions. Selected compositions of injection molded SRBSN were also studied using selected processing conditions. The results from the two fabrication techniques were compared.

The strength results are summarized in Table XIII. The results show that the strength of the dry pressed material is optimized when the sintering temperature was near the critical temperature. Here, the density was maximized while the microstructure remained fine and uniform. The fracture origins of these samples could not be identified, but a plot of strength versus volume fraction porosity, Fig. 20, for a number of compositions processed using these conditions show that the strength controlling defect is probably porosity. Samples processed in experiment 4 exhibited strengths of 133 Ksi and a Weibull modulus of 22. This represents a 35 percent increase in strength over the baseline value.

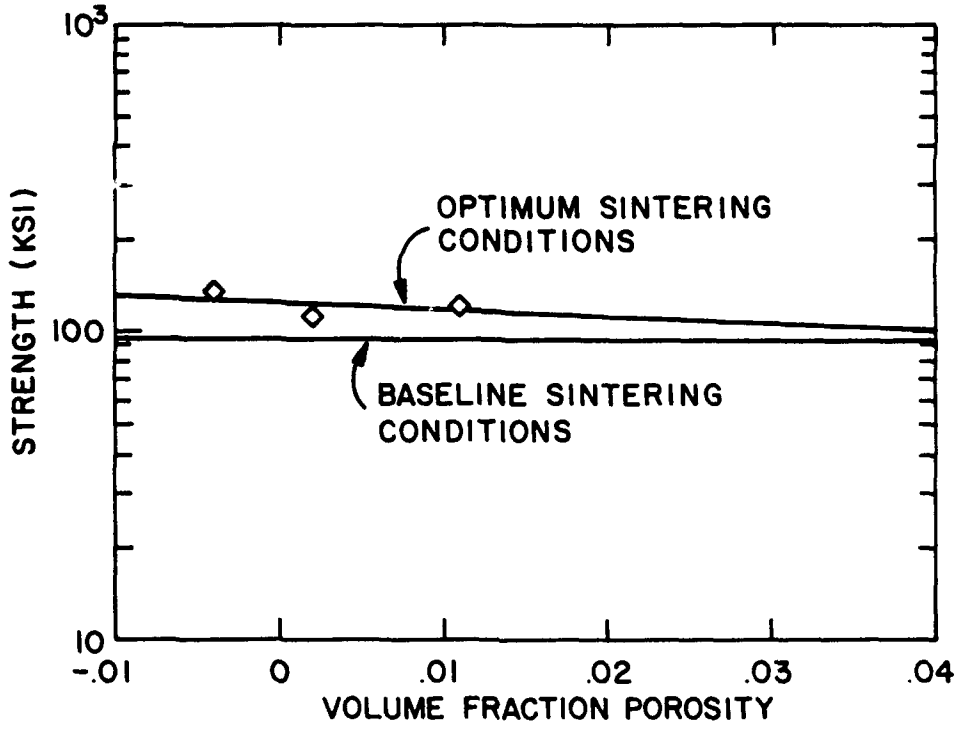

Fig. 20. *Strength versus volume fraction porosity for a SRBSN processed below the critical sintering temperature. The observed strength increase is due to an optimized microstructure.*

The injection molded SRBSN was processed using the baseline conditions and those of experiment 4. The strength of the molded material did not improve with the new sintering conditions. Analysis showed that the bulk microstructure was identical to the corresponding dry pressed material, Fig. 21, but the fracture origins were different. SEM analysis showed the strength controlling defects to be metallic inclusions of silicon and iron, Fig. 22.

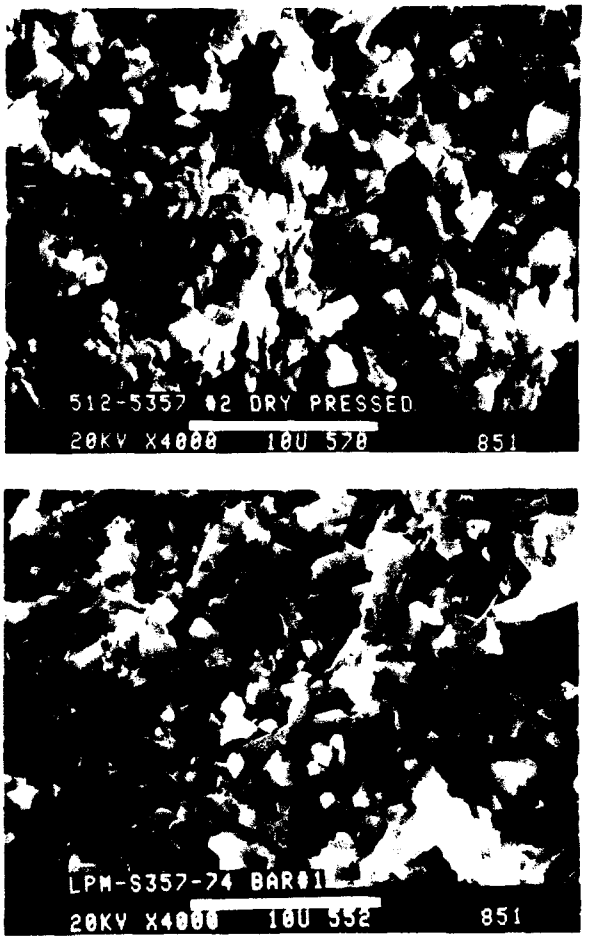

Fig. 21. Typical micrographs of dry pressed (A) and injection molded (B) SRBSN, processed using the "optimum" sintering cycle.

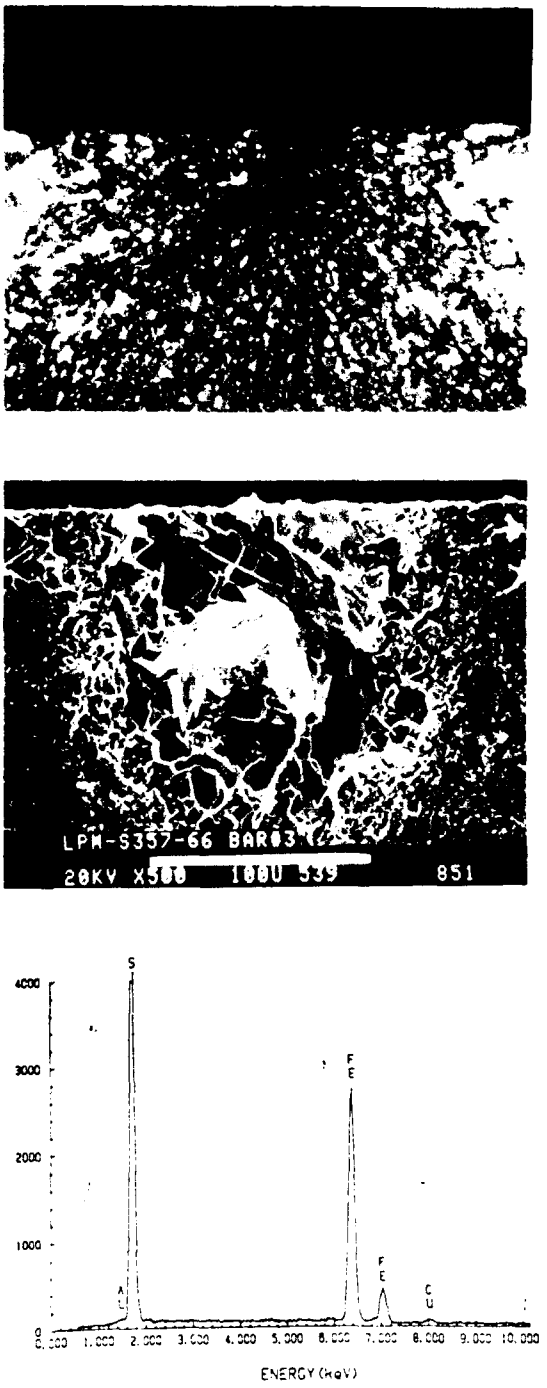

Fig. 22. Typical fracture origins of the injection molded SRBSN. Inclusions are compounds of iron and silicon.

F. Integral shaft spin disk (ISSD) mold design

The most critical aspect of injection molding a thick cross section component, like the ISSD, is the solidification behavior of the molding material in the die cavity. If solidification is

not controlled properly, internal voids and cracks occur. Heretofore, the control of the solidification behavior has been somewhat by chance. This important factor has not been considered in the design of tooling for injection molded silicon nitride components.

The solidification behavior of the molding material is controlled by the temperature of the material. The molding material solidifies with decreasing temperature. The last volume of material to solidify tends to have a void in it due to shrinkage. This volume is the last part to cool. A properly designed injection molding tool controls the temperature distribution with time so that the last volume to cool to the solidification temperature is in the sprue, and not in the part.

The purpose of this study was: (1) to apply conventional finite element techniques to model the temperature distribution with time of the injection molding material in an ISSD configuration, (2) iterate the tooling design using the model until the desired temperature distribution was obtained, and (3) fabricate the optimum tooling and confirm the model by producing ISSD components.

An axisymmetric finite element heat transfer program with transient temperature capabilities was used to study the temperature distribution with time of the injection molding material in the ISSD die cavity. The finite element model is shown in Fig. 23. The model simulates three parts of the ISSD injection molding die, the base, the cone section, and the cap, as well as the molding mix. The molding material includes two sections, the integral shaft spin disk, and the sprue. After molding the sprue is machined away, but at molding time the two parts are as one.

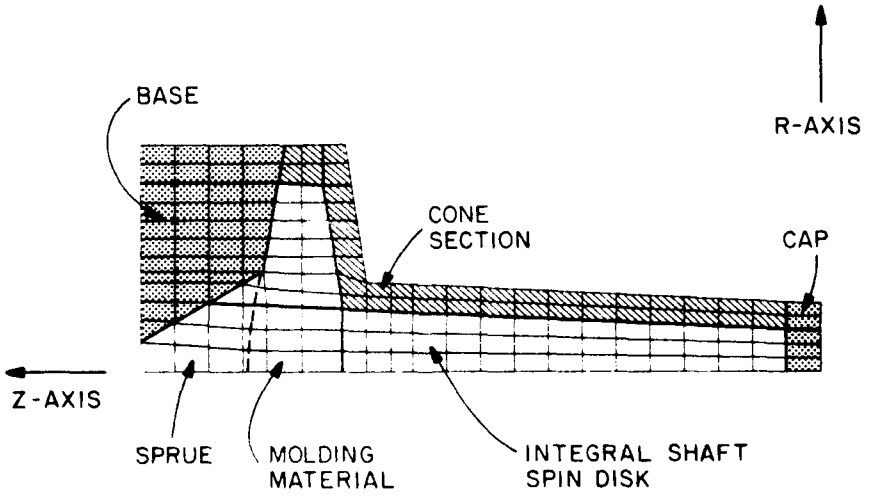

Fig. 23. ISSD injection molding die finite element model.

External to the die itself is a cooling system which is used to control the molding mix temperature as it is cooled. In this study air impingement and water cooling systems were studied. The hardware needed to implement the cooling system does not to be modeled, since it appears in the finite element model only as heat transfer coefficients.

The cooling of the molding mix and die was simulated with heat transfer calculations assuming a uniform initial die temperature was 100°F, and a uniform initial molding material was 215°F. These are reasonable assumptions since the die and the molding material are initially heated and their temperatures are monitored before molding a part. These are the target temperatures. The molding material must be heated before molding so that it flows freely, and the die must be at the proper temperature so that the incoming molding material does not stick to the die, interfering with the flow of the molding material into the die. The die is filled in a fraction of a second which further justifies uniform initial temperatures.

The temperature distribution two minutes after the die is filled is shown in Fig. 24. The die is being cooled with air impinging on the acute cone, and the die is sitting on the heater at a temperature of 180°F. There is a hot spot of 200°F in the middle of the disk region. If this cooling pattern continued a shrinkage void would result.

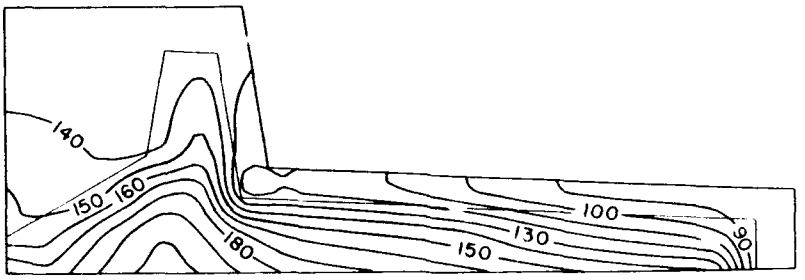

Fig. 24. Temperature distribution two minutes after filling.

Figure 25 illustrates the temperature distribution 14 minutes after filling assuming the die has been removed from the heater and sat on a large plate whose temperature is 75°F. The middle of the disk region is warmer than that of the rest of the part and it will solidify last, leaving a shrinkage void.

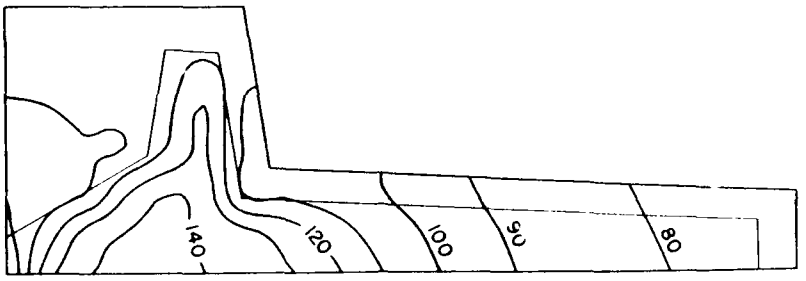

Fig. 25. Temperature distribution 14 minutes after filling, die removed from the heater.

This is the situation to be avoided. The die must be left on the heater, so that heat can be delivered to the die and molding material establishing the temperature distribution shown in Fig. 26. Here the temperatures are uniformly decreasing down the length of the part. Heat is flowing in from the base and out the acute cone. Continued cooling with this distribution will not leave any hot spots isolated in the interior of the part.

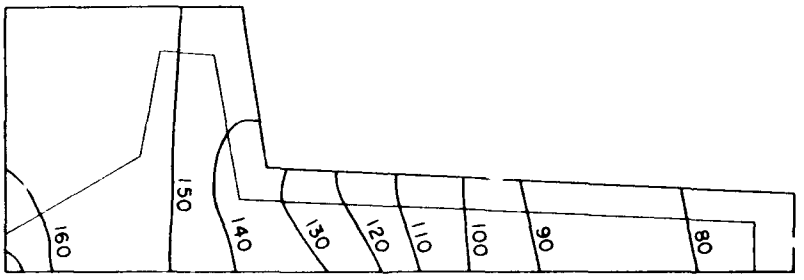

Fig. 26. Temperature distribution 10 minutes after filling.

To maintain a uniformly decreasing temperature distribution the heater temperature must be reduced while cooling is maintained on the cone. Fig. 27. illustrates the die at twenty minutes assuming the heater temperature was reduced to 160°F after ten minutes. The temperature distribution is still uniformly decreasing while the temperatures have dropped.

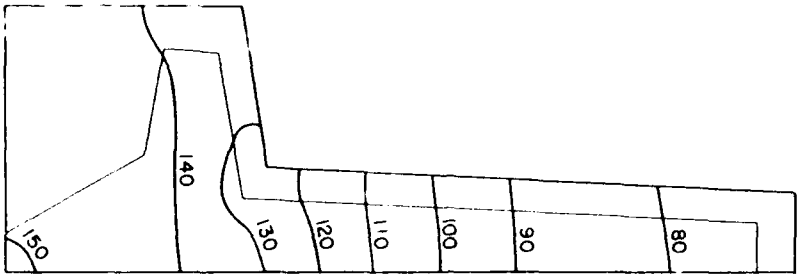

Fig. 27. Temperature distribution 20 minutes after filling.

Figure 28 illustrates the temperature distribution 30 minutes after filling assuming the heater temperature was reduced at 20 minutes to 140°F. The temperatures have now decayed to the point where the molding material has solidified and no hot spots have been left behind in the molding material's interior. At this point in time the die could be removed from the heater for some further cooling and the part could be removed from the die.

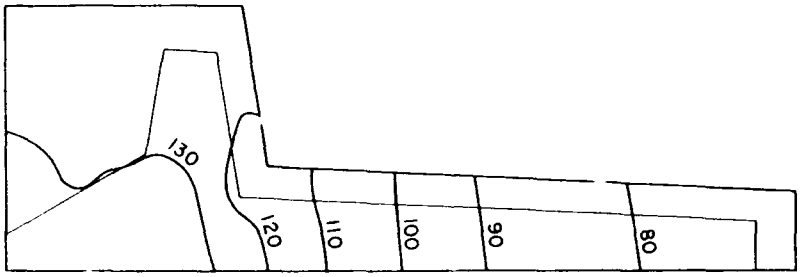

Fig. 28. Temperature distribution 30 minutes after filling.

Several temperature distributions versus time were calculated for cooling systems where the heater temperature was constant with time, but none of these gave the desired result of leaving no isolated hot spots in the molding mix interior. It appears that heater temperature control is necessary to achieve this result.

IV. ATTACHMENT DEVELOPMENT

A. Introduction

Two types of ceramic to metal attachments were developed to allow hot spin testing of integral shaft spin disks. Both attachments used the principle of a high thermal expansion plastic sleeve trapped in a relatively constant volume created between ceramic and steel shafts. One attachment uses a steel lock nut to trap the plastic, and the second uses a special type of thread on the ceramic shaft to trap the plastic.

Both these patented attachment designs were successfully and extensively tested in bench test rigs using several plastic and ceramic materials. Spin rig tests of the metal lock nut version ran slightly more than 80 hours in the hot spin rig. Two further versions of the screw on type attachment are presently under construction and a new version of the lock nut attachment is presently in test.

Early life prediction tests were conducted using spin disks machined from hot pressed billets of silicon nitride. These disks were mounted on a steel shaft using curvic couplings and an air cooled tie bolt[10,11]. The use of curvic couplings to attach a relative thin disk require a metal to ceramic attachment in a hot environment and the attachment may have high stresses. For life prediction testing this presents the potential of a failure due to the ceramic to metal attachment instead of a failure in the ceramic due to time dependent characteristics of the ceramic.

The casting of a spin disk, Fig. 29, with a six inch integral shaft made possible an attachment located in the bearing compartment. This is a relatively low temperature region and the attachment would have low stresses. The disk would run in an environment where it would be subjected to only thermal and centrifugal stresses. This would make a much more controlled test for life prediction testing.

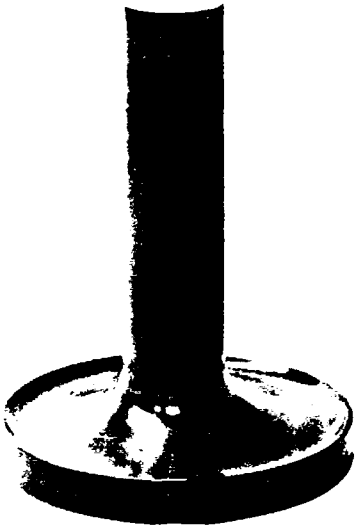

Fig. 29. Integral shaft rotor.

After some deliberation a design was conceived which used to advantage the relatively high thermal expansion rate of various plastics along with their softness compared to ceramics. The design concept lent itself to two configurations which were termed the non-threaded high expansion lock attachment and the threaded high expansion lock attachment. The non-threaded lock was the first design to be developed and will be reported first. The basic principle of operation is the same for both designs; however, the method of accomplishing this is different.

B. Non-threaded design high expansion lock

The most fundamental problem in joining ceramics with metals is their greatly differing thermal expansion rates. A ratio of 5 to 1 for steel and ceramic are not unusual. If joints of steel and ceramic are assembled and locked at a common temperature and then heated, strains quickly develop in the ceramic which can cause failures at very modest temperature excursions. For this reason attachment of metals to ceramics in areas subject to temperature variations is difficult. The idea of using a high expansion plastic sleeve, trapped in a volume formed by concentric shafts was first tested in a simple bench test rig shown in Fig 30.

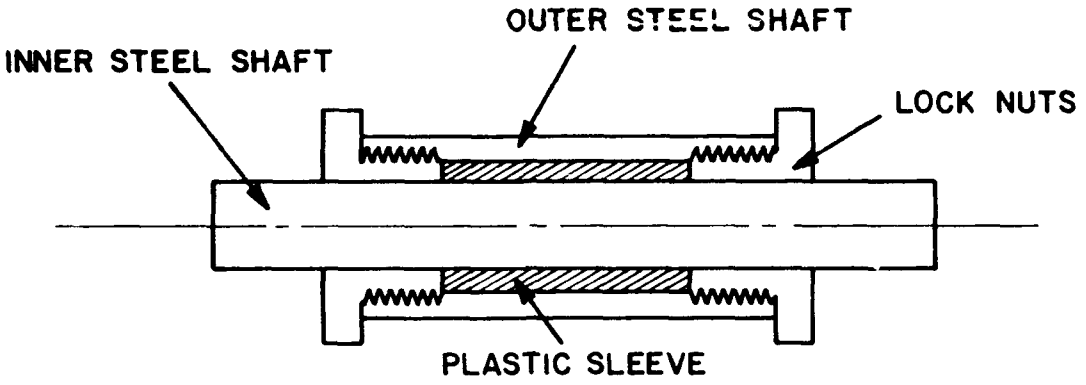

Fig. 30. First design non-threaded high expansion lock bench test rig.

This design trapped a nylon sleeve in the relatively constant volume chamber formed by inner and outer steel shafts and two end caps. Nylon, with linear expansion rate of 45 to 55×10^{-6}°F, would with increasing temperature, increase in volume much faster than the entrapping chamber. This volume expansion would create high pressure in the nylon sleeve, locking the two steel shafts. Steel was used for both shafts in the first design to simplify the fabrication problems. Also, to simplify the fabrication problem, the nylon sleeve and the inner steel shaft were slip fit at room temperature. This provided no locking at room temperature, a feature required for a successful attachment. The design would demonstrate the principle and room temperature locking could be incorporated into the design later.

The two end nuts, and the two shafts were made of cold rolled steel. The sleeve was nylon and the dimensions were sized to give the nylon sleeve a slip fit over the inner shaft and inside the outer shaft. The end nuts were screwed down tightly against the nylon. This assembly was heated to 180°F metal temperature and the shaft was pushed axially through the assembly. The break away load was 3200 pounds and constant motion was sustained at 2000 pounds. This test proved that the loads necessary to hold a rotor shaft assembly could be generated.

To accomplish room temperature locking, a new nylon sleeve was made that had a bore diameter 0.003 inches larger than the 0.750 inch diameter steel shaft. The outer diameter was 0.003 inch larger than the 1.000 inch inner diameter of the outer steel shaft. In order to assemble the parts, the inner shaft and the sleeve were soaked in a dry ice and alcohol bath until the sleeve had shrunk to a tight fit to the inner shaft and a slip fit to the outer shaft. The parts were then assembled and allowed to return to room temperature. Axial

break away load at room temperature was 800 pounds and the sliding load was 500 to 600 pounds. The parts were then heated to 300F in order to simulate rig temperatures and re-cooled. Examination of the parts at room temperature disclosed that the steel outer shaft had plastically yielded due to the high pressures generated. These initial bench tests proved that the idea would work but that the nylons' expansion rate was too high, generating a very rapid internal pressure rise when heated. Also, the inner steel shaft caused the entrapped volume to be smaller for a given temperature than an inner ceramic shaft would thus making the pressure rise even greater.

A new bench rig was designed that more closely simulated a ceramic to steel attachment as shown in Fig. 31. The outer steel shaft wall was increased in thickness for additional strength and a silicon nitride inner shaft, of NC-132, was substituted for the steel inner shaft to reduce the force on the nylon sleeve's internal diameter.

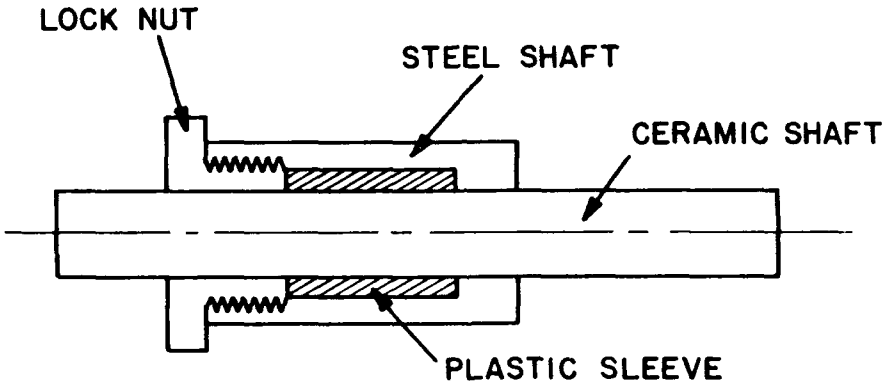

Fig. 31. Second design non-threaded high expansion lock bench test rig.

The test, after assembled parts came to room temperature, produced no motion between the parts at 3600 pounds axial load. This high load indicated that nylon was unsatisfactory as a sleeve material, since nylons' expansion rate would cause excessive pressures on the steel outer shaft at anticipated operated temperature.

A new sleeve of Celanese Plastic's Celcon GC-25 was fabricated. This plastics expansion rate was $22 \times 10^{-6}/^{o}F$ as compared to 45 to $55 \times 10^{-6}/^{o}F$ for nylon. The first test using Celcon GC-25 produced a room temperature break away load of 3400 pounds and at $140^{o}F$ the load rose to 4600 pounds. As a check against a plastic deformation of the steel, the assembly was heated to $300^{o}F$ and cooled. No deformation occurred and the assembly remained tight at room temperature.

This successful test lead to an invention disclosure and a patent application. Patent number 4,485,545 was awarded December 4, 1984.

One further area for improvement in the attachment design was to increase the service temperature of the plastic sleeve. A new product of Dupont, Vespel SP-22™, was selected which has a service temperature of 500°F and an expansion rate of $15x10^{-6}$ to $20x10^{-6}$/°F. Vespel SP-22™ is a 25% graphite filled polyimide resin with a bulk modulus of 475,000 psi. Its higher service temperature will give more temperature flexibility in the operation of high expansion locks.

With this last refinement to the attachment scheme it was decided to test a rotor in the hot spin rig and machining of a high expansion lock was begun on an integral shaft disk. A cross-section of the assembly is shown in Fig. 32. Figure 33 is a picture of the detail parts in the assembly plus the wrench necessary for assembly.

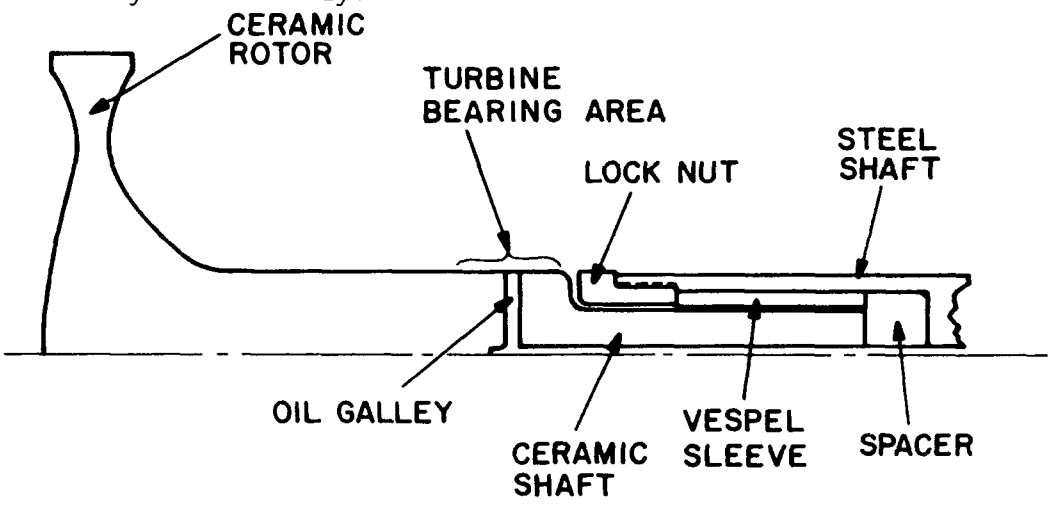

Fig. 32. Cross-sectional view of non-threaded high expansion lock rotor assembly.

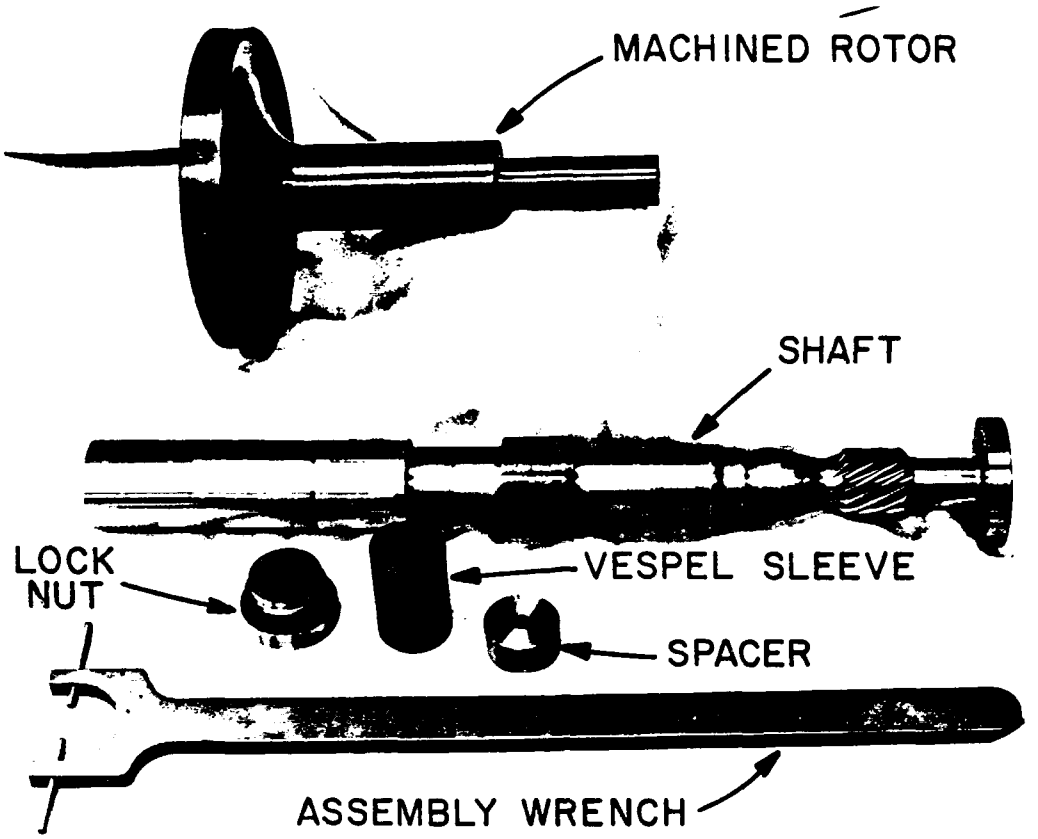

Fig. 33. Non-threaded high expansion lock rotor test parts.

The assembly was balanced to 0.001 inch-oz and installed into the hot spin rig. The initial testing consisted of nine short runs. After each run the rotor assembly was removed and checked balanced and visually inspected to see if any separation of the parts occurred. This series of tests proved the assembly to be stable, so an endurance test featuring increasing speeds and temperatures was begun. This test ended after 80 hours of testing when the rotor failed at 45,000 rpm and 1800°F rim temperature. The failure occurred in the ceramic part at the at the shoulder where the 0.750 diameter portion of the ceramic shaft blends into the 1.310 inch bearing diameter. The attachment section was still whole and had to be machined apart for inspection.

Careful inspection of the failed parts suggested that contact with the steel locking nut in the shoulder area where the failure occurred may have been a contributing factor. A simplifying redesign using a Vespel™ sleeve with a locking thread ground on the sleeve was fabricated and was tested. Figure 34 shows the part which takes the place of both the sleeve and lock nut shown in Fig. 32.

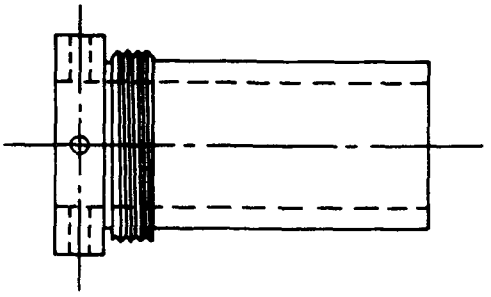

Fig. 34. All Vespel^{TM} combination lock and sleeve.

The all Vespel^{TM} combination lock and sleeve was evaluated with a Kyocera SN-220M integral shaft spin disk. Testing was conducted at 1500°F rim temperature. The initial test was at 2000 rpm for a period of one hour. The assembly was then inspected to make sure that no relative motion between the rotor and steel shaft had occurred. Testing was then conducted in 5 hour intervals, starting at 5000 rpm and going to 25000 rpm, in 5000 rpm increments. The assembly was inspected after each 5000 rpm increment. After these incremental tests, twenty and one-half hours of testing were conducted at 30000 rpm at a rim temperature of 1500°F. The combination lock and sleeve performed successfully.

C. Threaded design high expansion lock

In the non-threaded design, Fig. 32, the function of the lock nut is to form one of the entrapping volumes' walls. The rotor shaft is not axially locked in position by any mechanical means but it is frictionally locked to the entrapped plastic sleeve. The spacer plug is not necessary to the design but was used to make available hardware usable. The design thus requires two parts in addition to the two being joined.

In order to simplify the design further the function of the lock nut would have to be assumed by a shoulder on the ceramic shaft and the shaft would have to be locked to the steel rotor shaft. To accomplish this a threaded ceramic to steel attachment was designed, Fig. 35. In this design the rotor to metal joint requires only one additional part to accomplish attachment and that is the plastic sleeve. In assembly the rotor and sleeve are cooled and screwed into the rotor shaft until the sleeve is axially trapped. This design was granted a patent, number 4,499,646, in February 1985.

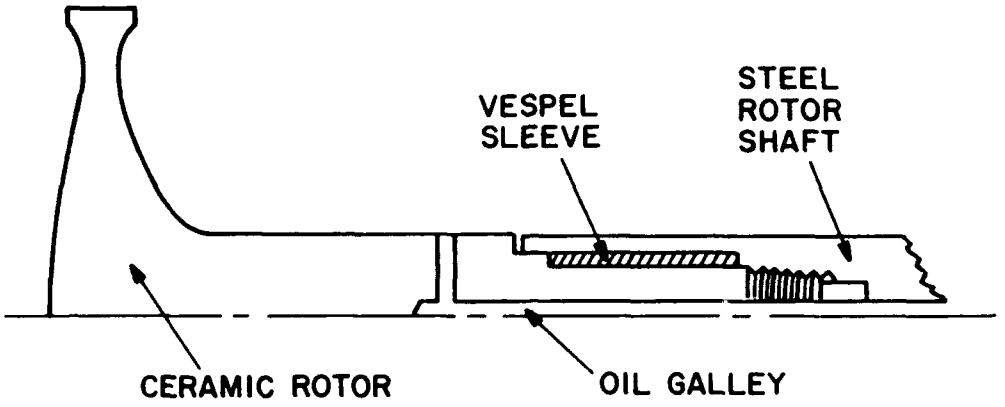

Fig. 35. Threaded ceramic to steel attachment.

Parts for a hot spin rig test were fabricated. The individual parts and the assembly are shown in Fig. 36. The test was conducted at low speed, 2000 rpm and the rim temperature of the rotor set at 2000°F as measured by a radiation pyrometer. After 15 minutes of testing a failure occurred in the thread portion of the rotor shaft. Failure analysis of the parts suggested that the metal had bridged the front and rear face of two separate threads and put the thread section in tension, causing a failure in the thread root. The threads used in this design were standard 60 degree vee threads. Two possible problems were considered as causing the failure: (1) excessive high pressures in the plastic sleeve which would cause excessive tensile loads on the ceramic threads, and (2) a dimensional mismatch between the ceramic and steel threads which would cause excessive stresses in the ceramic threads. A bench test was designed to try and duplicate the hot spin rig failure and allow a convenient way to test changes in thread designs to overcome the problem. The bench rig is shown in Fig. 37.

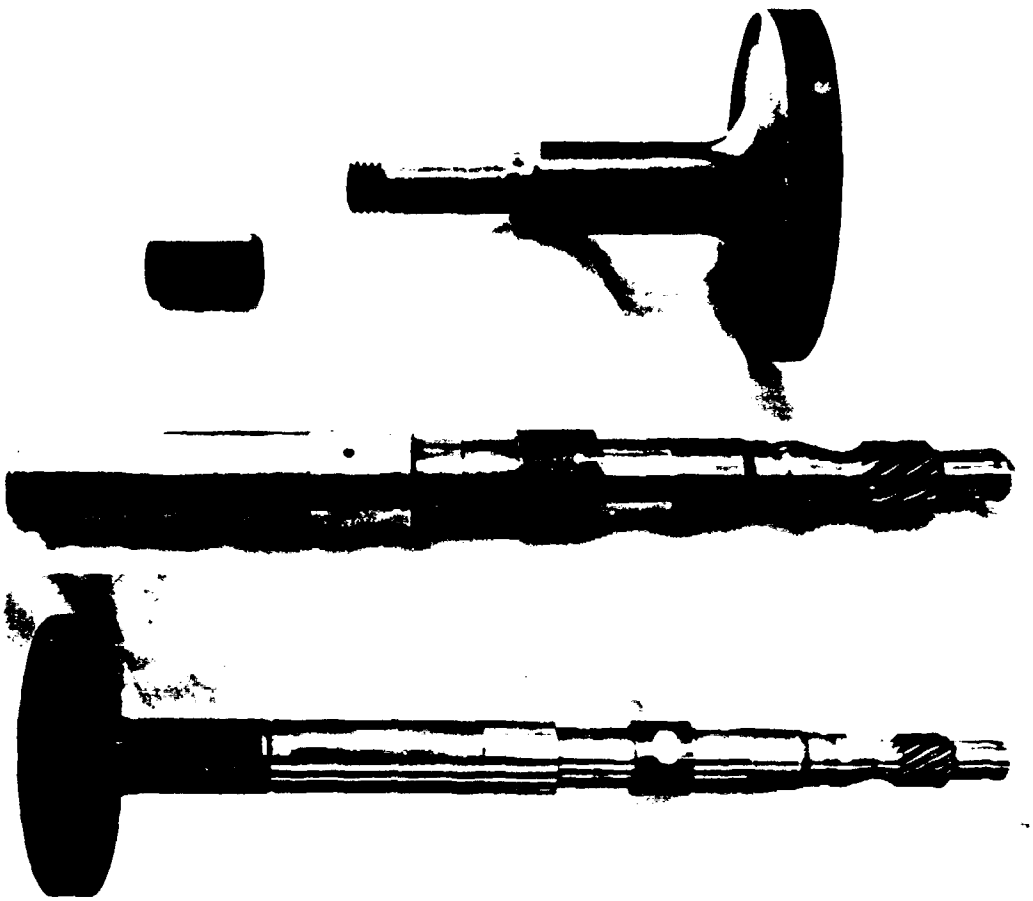

Fig. 36. Threaded attachment test parts and assembly.

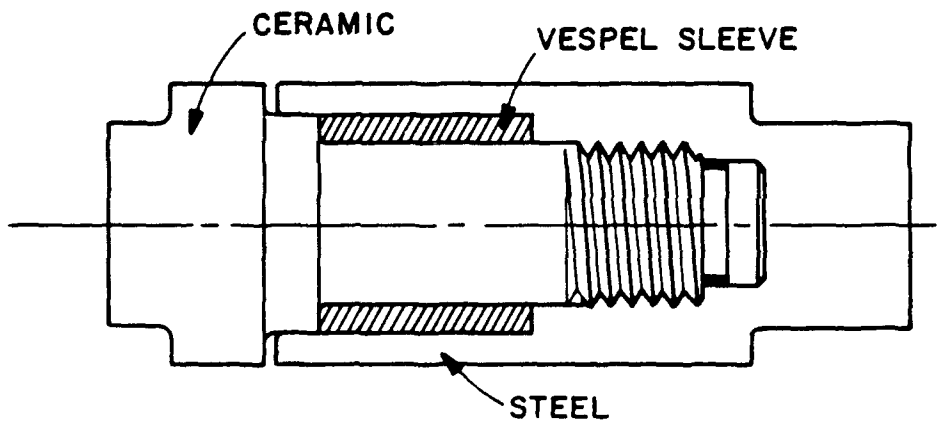

Fig. 37. Bench test rig screw thread attachment.

In order to also generate some information on the pressure rise inside the assembly. Three strain gages were placed on the outer diameter of the steel part. The gages were temperature compensated and were thermally cycled three times to guarantee stable readings. The ceramic part was made from GTE's SNW-1000, this material was used because of its available. The steel part was cold rolled steel. A thermal cycle test produced a failure on the first cycle at 210°F. metal temperature at an internal pressure of 1400 to 1600 psi. The failure occurred at temperature just a few degrees above the normal oil temperature used in the hot spin rig and the test appeared to give a very good correlation to the failure of the actual rotor test. The failed assembly is shown in Fig. 38.

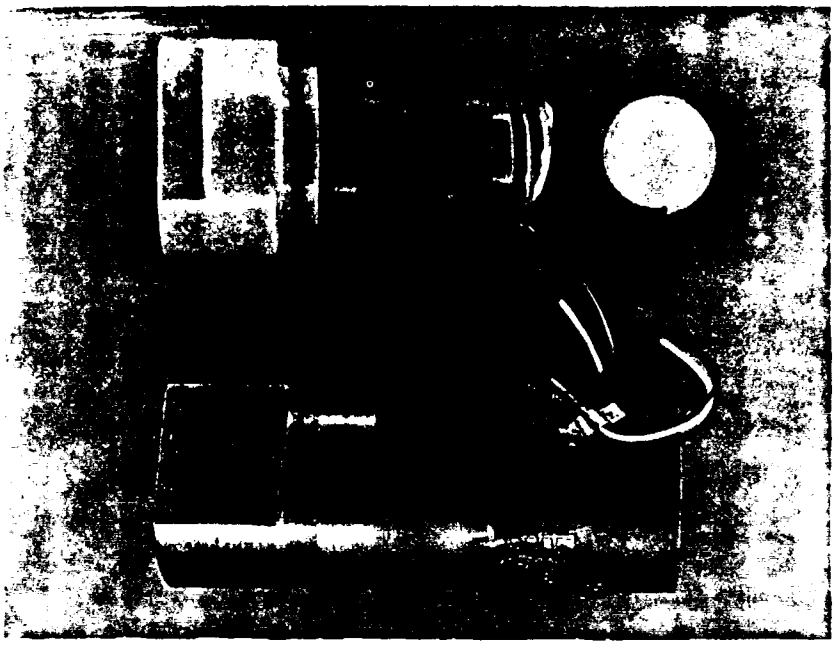

Fig. 38. Failed bench test rig.

The pressure produced during this test was not high enough to overload the ceramic threads in tension; hence, the problem appeared to be due to axial thread interference and subsequent tension in the ceramic caused by expanding metal. A thread design was sought which would prevent this by assuring sufficient clearance on the unloaded side of the thread. This was provided by a buttress thread whose basic form is show in Fig. 39.

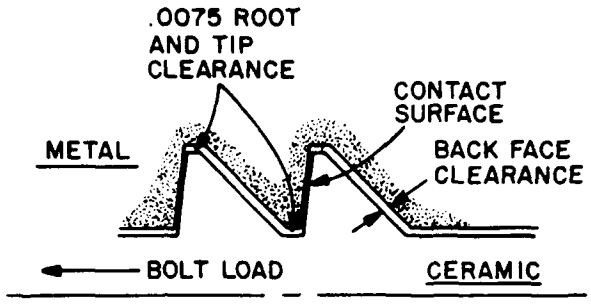

Fig. 39. Buttress thread form.

Included in this second screw thread rig test was a tapered Vespel^{TM} sleeve. The outside sleeve diameter was tapered toward the threaded end of ceramic. This change was to aid assembly. With a straight cylindrical sleeve, assembly was difficult because the parts, as cooled, are slightly under a line to line fit. Assembly has to be accomplished quickly or the joint tends to lock up while half assembled. A 2 degree taper on the outside of the sleeve enables the assembly to be almost completely secured before the mating parts touch and begin to lock up. This modification eased the assembly by permitting most of the threads to engage before the Vespel^{TM} sleeve came in contact with the steel and began to expand.

The steel shaft was strained gaged as in the previous test. An attempt was made to assemble the parts. However, the parts began to lock up before the threads were fully engaged. Torque was applied to the ceramic head to drive the Vespel^{TM} fully into the sleeve cavity but the SNW-1000 material failed at the thread as shown in Fig. 40. Since this material with its room temperature modulus of rupture of 95000 psi, wasn't going to stand up to the rigors of assembly, a new ceramic part was made from NC-132, a hot pressed silicon nitride.

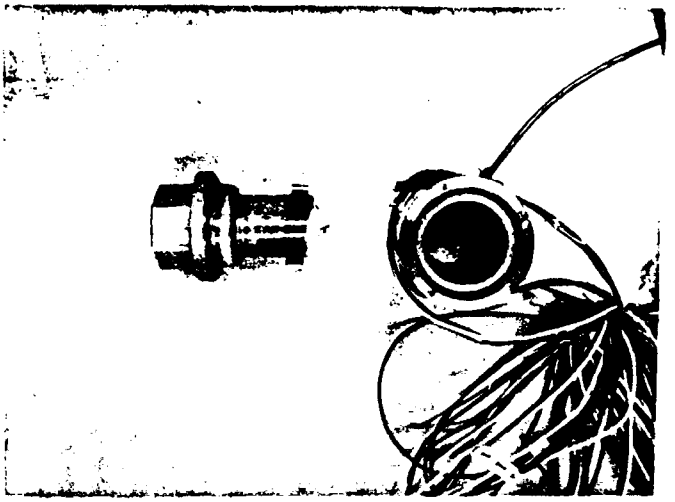

Fig. 40. Buttress thread test rig, SNW-1000.

This part, along with the sleeve and strain gaged outer steel shaft, are shown in Fig. 41. They were successfully assembled. The thermal cycle test began after the assembly had normalized at room temperature for 24 hours. Before assembly the strain gage pots had been zeroed with the steel case unstrained. The pots were not adjusted during the rest of the test. The gage readings were noted before the assembly was heated and are shown in Table XIV. The assembly was slowly heated to 290°F and then to 341°F where it was allowed to remain overnight. The readings were recorded, the assembly cooled to room temperature and the final readings taken. The gages readings were averaged and converted to stress assuming the Young's modulus was 30×10^6 psi. The stress values were then used to approximate the internal pressure using Eqn. 1.

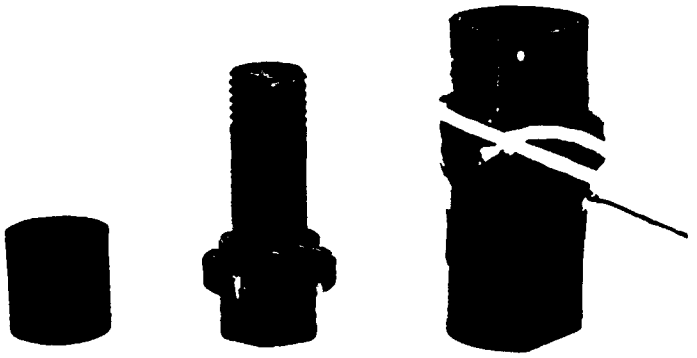

Fig. 41. NC-132 Buttress thread rig parts.

$$\sigma_T = \frac{P}{b^2 a^2} \left(1 + \frac{b^2}{R^2} \right) \qquad (1)$$

where

σ_T = hoop stress(psi)
P = internal pressure,psi
b = External radius,inches (0.655)
a = Internal radius,inches (0.500)
R = Radius where stress is to be calculated,inches (0.655)

Equation 1 reduces to Eqn. 2.

$$\sigma_T = 11.17\ P \qquad (2)$$

Or solving for pressure.

$$P = 0.089\ \sigma_T \qquad (3)$$

This formula is used to predict stress in thick walled tubes and the rig part doesn't strictly meet the requirements of open

soak were very consistent. After this first test the gages were glass beaded off the outer steel shaft and the assembly is shown in Fig. 42.

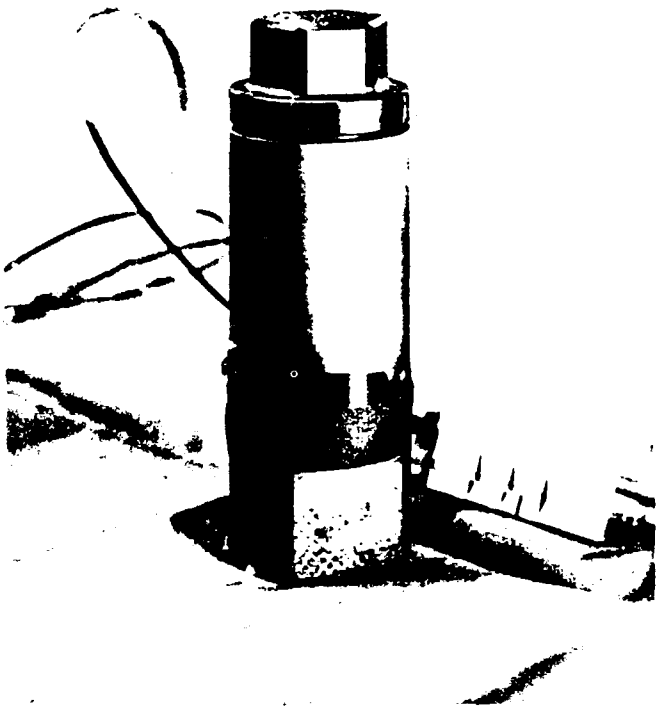

Fig. 42. NC-132 Buttress thread test rig assembly.

A second test was conducted to see how the diameter of the assembly changed with temperature. The data appears in Fig. 43. This data shows that the diameter expands at a rate consistent with a linear thermal expansion coefficient of 8 or $9x10^{-6}$ inches per inch per degrees Fahrenheit which is a representative value for steels. The plastic sleeve pressure contributes little to the outer steel shaft expansion. This data is useful if a joint were made in the area of a bearing where increases in diameter would have to be predicted so sufficient cold clearances could be built in.

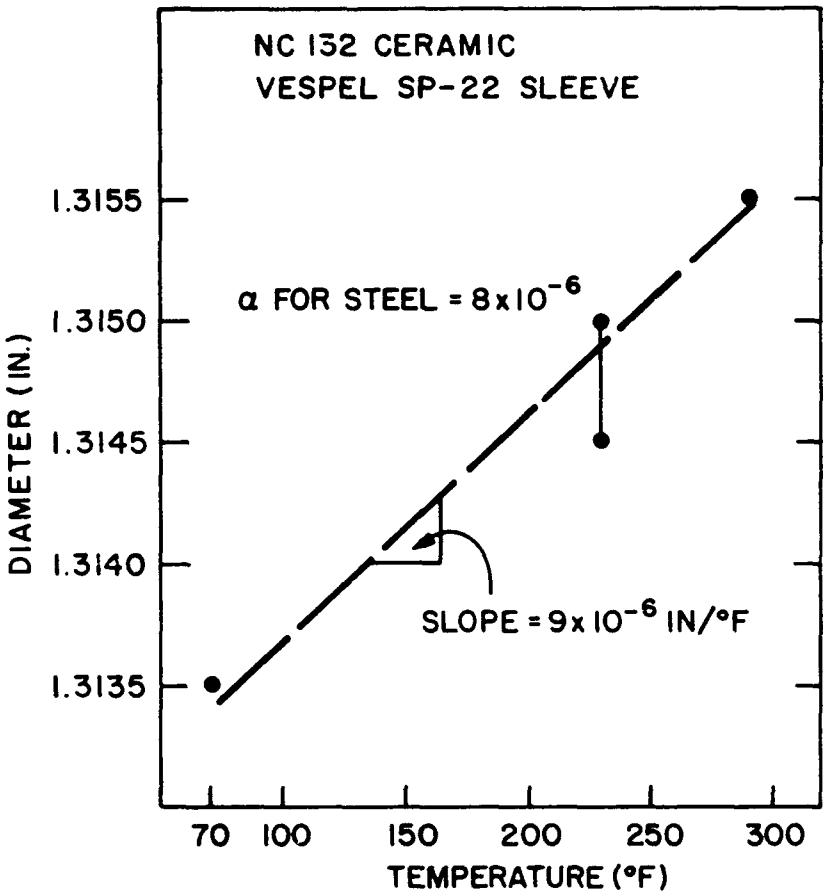

Fig. 43. Assembly diameter increase versus temperature.

After the final diameter versus temperature test, an attempt was made to unscrew the ceramic part. The parts were tightly held together and it was necessary to machine a groove around the steel portion to allow the threads to unscrew without turning the ceramic relative to the sleeve. After final disassembly several of the ceramic threads were found to be chipped. There were some chips at assembly, but the further damage was probably caused by a chip type failure occurring at assembly with that loose chip jamming and causing much more damage upon disassembly. The steel sleeve still surrounding the Vespel™ and the ceramic had to be pressed apart in a special fixture. The parts and the fixture are shown in Fig. 44.

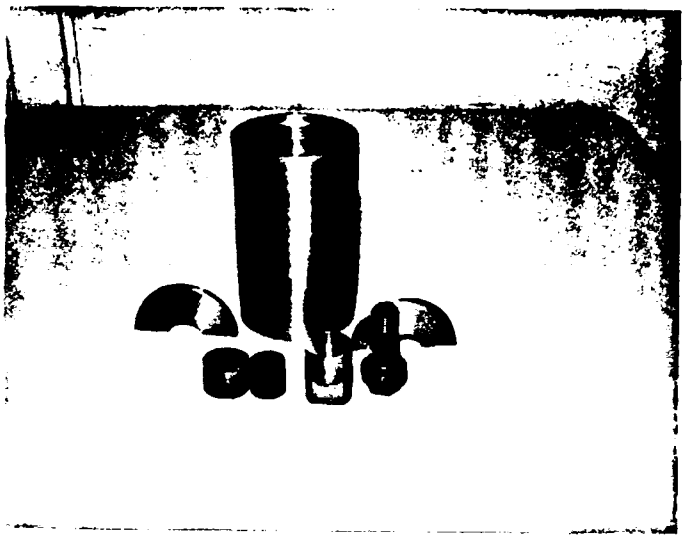

Fig. 44. Disassembled NC-132 buttress thread rig.

Recent efforts have been directed at reducing the chipping tendency of the very thin edge of the 3/4-12 buttress threads first used. Taps have been purchased to cut 3/4-8 buttress threads and a 3/4-6 Acme thread (29 degrees face angle). Diamond plated grinding wheels to produce these threads on the ceramic test parts are also being purchased. The present plan is to test an Acme threaded attachment in the hot spin rig with the final design of this program as shown in Fig. 45.

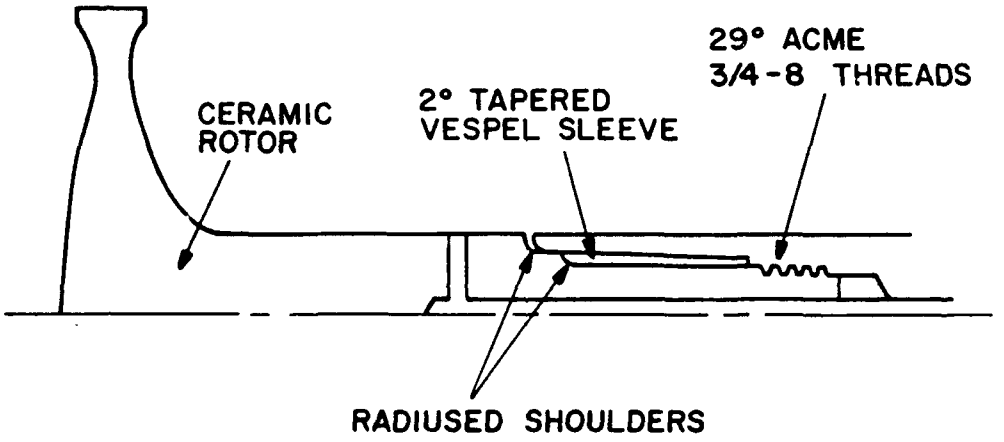

Fig. 45. Threaded attachment final design.

V. SUMMARY

The original intent of this phase of the Life Prediction Methodolgy Program was to repeat the stress rupture tests conducted on NC-132 disks with a second material in order to verify the life prediction methods developed under that phase of the program. These tests were to be conducted with integral shaft spin disks. The integral shaft design was to make possible a simpler and more reliable attachment than that used with the NC-132 disks. The program was to characterize the integral shaft spin disk material in order determine the test conditions for the spin disk. The assumption was that the material was reproducible. As the characterization commenced it became apparent that the material was not reproducible; therefore, the program was modified to include a period of specimen development after which the characterization and testing would be resumed. Curtailment of the funding precluded the completion of all the tasks.

Initial characterization testing was conducted on a sintered silicon nitride supplied by Ford. Fast fracture testing was conducted at room temperature on ten specimens in four point bending. The fracture strength varied from a minimum of 785 MPa to a maximum of 988 MPa with an average strength of 873 MPa, and a standard deviation of 79 MPa with a Weibull modulus of 13. Stress rupture testing was conducted in the intermediate temperature range of 600°C to 1000°C to determine if the material was instable in this range. Two specimens were tested at a stress level of 344 MPa. One survived 306 hours without failure of bending while the second specimen failed in 35 hours. Examination of the fracture surface of the second specimen revealed the presence of a locally oxidized region as the failure initiation source. A third specimen was tested at 413 MPa. It failed in one hour. The behavior of these three specimens and others tested indicated that the material has an instability at 1000°C. At this point the program was reviewed and modified to include a period of specimen development.

The objective of the specimen development part of the program was to develop the methodology to fabricate the integral shaft spin disk with reproducible properties, using an injection molded, sintered reaction bonded silicon nitride. After the specimen development was completed the program was to resume the material characterization and spin testing phases of the program. The specimen development was divided into two major areas: (1) injection molding, and (2) sintering-property development.

A set of statistically designed experiments was performed to relate the effect of four injection molding variables to component quality after injection molding and after binder removal from the injection molded part. The experiments evaluated the effect of four injection molding variables on part quality after molding and after binder removal. The injection molding

variables were die temperature, injection pressure, material temperature, and hold time. A 2^{4-1} fractional factorial experimental design was employed. The experiment was repeated for two components. Two responses were considered critical after molding: (1) density, and (2) the number of x-ray indications. The quality parameters relating to cracks are only important after binder removal. The results generally indicated that all four injection molding variables, die temperature, injection pressure, material temperature, and hold time should be reduced in order to improve the component quality. They showed that conditions which are thought to a yield low stress state in the component also result in a high quality component after molding and binder removal. They also showed that the molding conditions directly effect the quality of the component after binder removal.

A set of statistically designed experiments was performed to determine the effect of three binder removal processing variables on the component quality after binder removal. The variables investigated were (1) the pressure of the binder removal atmosphere, (2) the rate of temperature rise, and (3) the complexity of the geometry of the component. A full factorial 2^3 experimental design was employed to determine primary effects as well as interaction effects. The results indicated that higher binder removal percentages are obtained at high pressure than under low pressure conditions. This was found to be true for both large and small components. The results also indicated that the large component exhibits higher binder removal percentages than the small component. The results also indicated that there is an interaction between the heating rate and the pressure of the binder removal atmosphere.

In the sintering-property development two particular things were studied. These were (1) the microstructure development, and (2) strength improvements. Analysis of the microstructures of a number of compositions in the yttria/alumina system showed that a critical temperature exists above which exaggerated grain growth occurs and below which a uniform microstructure can be obtained. Sintering time above the critical temperature was identified as the principal parameter contributing to excessive grain growth. Sintering experiments above and below the critical temperature were conducted to determine maximum grain size and number of large grains per unit area versus time. The results defined a set of acceptable time-temperature sintering parameters required for obtaining a uniform microstructure in a sintered reaction bonded silicon nitride.

A set of experiments were conducted to improve the strength of the sintered reaction bonded silicon nitride. Dry pressed compositions were sintered using four sets of processing conditions where the sintering temperature and time were varied. They included a baseline where the sintering temperature was

above the critical temperature for grain growth and the time was long. The others included a short time at high temperature, long time at low temperature and an intermediate time and temperature. These last three sintering conditions were designed to generate a microstructure free of the large needle shaped grains. The density, strength and microstructure was studied for the four conditions. The results showed that the strength of the dry pressed material is optimized when the sintering temperature was near the critical temperature. This produced maximum density and a fine, uniform microstructure.

In addition to the control of the microstructure and strength of the molding material, the injection molding die used to form the integral shaft disk requires careful design. The die must be designed to control the solidification behavior of the molding material. The molding material solidifies and undergoes shrinkage with decreasing temperature. A properly designed injection molding tool controls the temperature distribution within the die such that the last volume to cool to the solidification temperature is in the sprue, and not in the part. This eliminates any possibility of the formation of shrinkage voids within the component. A finite element heat transfer study was conducted on a proposed integral shaft spin disk die. Temperature contours were plotted versus time for several different cooling designs. It was determined that in order to properly control the cooling of the molding material an active temperature control was required. The die must have a heater on the sprue end of the die, and the output of the heater must be reduced with time.

The integral shaft spin disk required the design and development of a new type attachment which would take advantage of the long ceramic shaft on the disk to locate the ceramic to metal attachment in a relatively cool location. This would increase the reliability of the attachment. Two types of ceramic to metal attachments were developed . Both attachments used the principle of a high thermal expansion plastic sleeve trapped in a relatively constant volume created between ceramic and steel shafts. One design used a steel lock nut to trap the plastic, and the second used a special type of thread on the ceramic shaft to trap the plastic. The designs were extensively tested in bench test rigs using several plastic and ceramic materials. The metal lock nut version was tested for more than 80 hours in the hot spin rig.

VI. CONCLUSIONS

A. The four injection molding variables, die temperature, injection pressure, material temperature, and hold time should be reduced in order to improve the component quality.

B. Binder removal rates from injection molded parts are improved with the use of a pressurized atmosphere.

C. A pressurized binder removal atmosphere increases component quality.

D. An active temperature control is required for injection molding an integral shaft disk.

E. The high expansion lock ceramic-to-metal attachment is suitable for use in a hot spin rig application.

TABLE I

Flexural Stress Rupture Results for Billet A-42

Temperature °C	Applied Stress MPa	Failure Time Hours	Suspension Time Hours	Remarks
800	413	-	336	Color changed to light gray, no spot formation
800	482	88	-	LOR, Color gray, no spot formation and no bending
1000	344	35	-	LOR, Uniform oxidation, Color white, no spot formation and no bending
1000	344	-	306	Color white, no spot formation and no bending
1000	413	1	-	Oxidation pit, Color whitish gray, no spot formation and no bending
1000	482	0.5	-	Porosity, Color whitish gray, no spot formation and no bending

LOR = Local Oxidation Region

TABLE II

Fast Fracture Strength Data for LAS at Room Temperature

Specimen Number	Fracture Strength MPa	Specimen Number	Fracture Strength MPa	Specimen Number	Fracture Strength MPa
1	114	11	143	21	127
2	127	12	130	22	125
3	156	13	156	23	116
4	130	14	130	24	128
5	125	15	126	25	118
6	142	16	130	26	99
7	143	17	129	27	134
8	156	18	142	28	139
9	141	19	137	29	143
10	161	20	121	30	130

TABLE III

Flexural Stress Rupture Results for LAS

Specimen Number	Temperature °C	Applied Stress MPa	Suspension Time Hours	Fracture Stress MPa	Remarks
31*	20	93(Fracture)			Specimen failed at pre-crack site, Fig. 3.
32*	20	114(Fracture)			Specimen failed at pre-crack site.
33	871	40	93	134	Did not fail at the pre-crack site.
34	871	40	50	137	Did not fail at the pre-crack site.
35	927	40	50	125	Did not fail at the pre-crack site.
36	927	40	50	116	Did not fail at the pre-crack site.
37	982	40	50	116	Failed at the precrack site and the semi-circular crack front is visible, Fig. 3.
38	982	40	50	116	Did not fail at the pre-crack site.
39	982	40	50	125	Did not fail at the pre-crack site.
40	982	40	50	109	Did not fail at the pre-crack site.

* Tested in fast fracture mode in order to reveal material's strength containing a precrack.

TABLE IV

LAS Thermal Stability Tests Results

BLOCK SERIAL NUMBER 1
TEST TEMPERATURE 1600 DEG-F

TOTAL TIME AT TEMPERATURE

FACE AND LOCATION OF DIMENSION	0 HOURS INCHES	285 HOURS INCHES	500 HOURS INCHES	1000 HOURS INCHES	SAMPLE RANGE INCHES
XA	1.00078	1.00078	1.00077	1.00078	0.00001
XB	1.00119	1.00119	1.00118	1.00114	0.00005
XC	1.00112	1.00108	1.00107	1.00102	0.00010
XD	1.00085	1.00088	1.00084	1.00082	0.00006
XE	1.00124	1.00125	1.00122	1.00122	0.00003
YA	1.00058	1.00057	1.00058	1.00056	0.00002
YB	1.00035	1.00030	1.00032	1.00030	0.00005
YC	1.00052	1.00053	1.00057	1.00050	0.00007
YD	1.00063	1.00045	1.00068	1.00060	0.00023
YE	1.00046	1.00033	1.00036	1.00035	0.00013
ZC	0.69692	0.69698	0.69692	0.69693	0.00006
WEIGHT GRAMS	26.7464	26.7457	26.7461	26.7462	0.0007

BLOCK SERIAL NUMBER 2
TEST TEMPERATURE 1600 DEG-F

TOTAL TIME AT TEMPERATURE

FACE AND LOCATION OF DIMENSION	0 HOURS INCHES	285 HOURS INCHES	500 HOURS INCHES	1000 HOURS INCHES	SAMPLE RANGE INCHES
XA	1.00062	1.00067	1.00063	1.00062	0.00005
XB	1.00092	1.00088	1.00087	1.00088	0.00005
XC	1.00073	1.00070	1.00077	1.00082	0.00012
XD	1.00055	1.00058	1.00057	1.00056	0.00003
XE	1.00082	1.00085	1.00084	1.00086	0.00004
YA	1.00047	1.00058	1.00048	1.00050	0.00011
YB	1.00055	1.00054	1.00052	1.00054	0.00003
YC	1.00057	1.00060	1.00057	1.00057	0.00003
YD	1.00060	1.00063	1.00059	1.00055	0.00008
YE	1.00066	1.00067	1.00067	1.00063	0.00004
ZC	0.69685	0.69714	0.69682	0.69684	0.00032
WEIGHT GRAMS	26.7309	26.7307	26.7307	26.7309	0.0002

BLOCK SERIAL NUMBER 3
TEST TEMPERATURE 1600 DEG-F

TOTAL TIME AT TEMPERATURE

FACE AND LOCATION OF DIMENSION	0 HOURS INCHES	285 HOURS INCHES	500 HOURS INCHES	1000 HOURS INCHES	SAMPLE RANGE INCHES
XA	1.00055	1.00055	1.00059	1.00050	0.00009
XB	1.00097	1.00096	1.00102	1.00099	0.00006
XC	1.00073	1.00081	1.00077	1.00075	0.00008
XD	1.00046	1.00038	1.00039	1.00038	0.00008
XE	1.00087	1.00087	1.00081	1.00083	0.00006
YA	1.00102	1.00098	1.00100	1.00100	0.00004
YB	1.00043	1.00037	1.00044	1.00040	0.00007
YC	1.00067	1.00065	1.00063	1.00067	0.00004
YD	1.00078	1.00075	1.00077	1.00072	0.00006
YE	1.00036	1.00012	1.00017	1.00013	0.00024
ZC	0.69677	0.69688	0.69675	0.69677	0.00013
WEIGHT GRAMS	26.7325	26.7321	26.7321	26.7324	0.0004

BLOCK SERIAL NUMBER 4
TEST TEMPERATURE 1600 DEG-F

TOTAL TIME AT TEMPERATURE

FACE AND LOCATION OF DIMENSION	0 HOURS INCHES	285 HOURS INCHES	500 HOURS INCHES	1000 HOURS INCHES	SAMPLE RANGE INCHES
XA	1.00047	1.00044	1.00045	1.00047	0.00003
XB	1.00080	1.00082	1.00074	1.00077	0.00008
XC	1.00053	1.00055	1.00057	1.00063	0.00010
XD	1.00014	1.00013	1.00016	1.00013	0.00003
XE	1.00054	1.00053	1.00052	1.00050	0.00004
YA	1.00055	1.00060	1.00057	1.00055	0.00005
YB	1.00112	1.00111	1.00117	1.00112	0.00006
YC	1.00091	1.00097	1.00100	1.00095	0.00009
YD	1.00054	1.00057	1.00055	1.00055	0.00003
YE	1.00110	1.00111	1.00109	1.00112	0.00003
ZC	0.69693	0.69714	0.69688	0.69688	0.00026
WEIGHT GRAMS	26.7259	26.7256	26.7257	26.7257	0.0003

BLOCK SERIAL NUMBER 5
TEST TEMPERATURE 1600 DEG-F

TOTAL TIME AT TEMPERATURE

FACE AND LOCATION OF DIMENSION	0 HOURS	285 HOURS	500 HOURS	1000 HOURS	SAMPLE RANGE
	INCHES	INCHES	INCHES	INCHES	INCHES
XA	1.00116	1.00114	1.00112	1.00115	0.00004
XB	1.00096	1.00092	1.00091	1.00092	0.00005
XC	1.00102	1.00102	1.00101	1.00104	0.00003
XD	1.00117	1.00114	1.00113	1.00130	0.00017
XE	1.00094	1.00095	1.00094	1.00090	0.00005
YA	1.00088	1.00088	1.00088	1.00083	0.00005
YB	1.00085	1.00083	1.00086	1.00083	0.00003
YC	1.00092	1.00093	1.00087	1.00089	0.00006
YD	1.00090	1.00091	1.00086	1.00088	0.00005
YE	1.00090	1.00082	1.00081	1.00082	0.00009
ZC	0.69685	0.69708	0.69698	0.69692	0.00023
WEIGHT GRAMS	26.7683	26.7677	26.7675	26.7676	0.0008

BLOCK SERIAL NUMBER 6
TEST TEMPERATURE 1700 DEG-F

TOTAL TIME AT TEMPERATURE

FACE AND LOCATION OF DIMENSION	0 HOURS	285 HOURS	500 HOURS	1000 HOURS	SAMPLE RANGE
	INCHES	INCHES	INCHES	INCHES	INCHES
XA	1.00079	1.00078	1.00080	1.00082	0.00004
XB	1.00059	1.00054	1.00052	1.00052	0.00007
XC	1.00078	1.00077	1.00086	1.00084	0.00009
XD	1.00096	1.00095	1.00094	1.00096	0.00002
XE	1.00073	1.00072	1.00082	1.00078	0.00010
YA	1.00071	1.00071	1.00081	1.00080	0.00010
YB	1.00064	1.00061	1.00062	1.00063	0.00003
YC	1.00077	1.00077	1.00085	1.00090	0.00013
YD	1.00081	1.00082	1.00079	1.00083	0.00004
YE	1.00075	1.00076	1.00085	1.00083	0.00010
ZC	0.69677	0.69682	0.69682	0.69682	0.00005
WEIGHT GRAMS	26.7259	26.7258	26.7255	26.7256	0.0004

BLOCK SERIAL NUMBER 7
TEST TEMPERATURE 1700 DEG-F

TOTAL TIME AT TEMPERATURE

FACE AND LOCATION OF DIMENSION	0 HOURS	285 HOURS	500 HOURS	1000 HOURS	SAMPLE RANGE
	INCHES	INCHES	INCHES	INCHES	INCHES
XA	1.00102	1.00094	1.00098	1.00094	0.00008
XB	1.00098	1.00096	1.00095	1.00097	0.00003
XC	1.00102	1.00088	1.00097	1.00085	0.00017
XD	1.00080	1.00075	1.00077	1.00068	0.00012
XE	1.00078	1.00077	1.00074	1.00074	0.00004
YA	1.00083	1.00086	1.00087	1.00092	0.00009
YB	1.00070	1.00071	1.00107	1.00068	0.00039
YC	1.00079	1.00081	1.00100	1.00082	0.00021
YD	1.00077	1.00079	1.00079	1.00070	0.00009
YE	1.00063	1.00063	1.00072	1.00058	0.00014
ZC	0.69677	0.69682	0.69686	0.69693	0.00016
WEIGHT GRAMS	26.7298	26.7295	26.7274	26.7296	0.0024

BLOCK SERIAL NUMBER 8
TEST TEMPERATURE 1700 DEG-F

TOTAL TIME AT TEMPERATURE

FACE AND LOCATION OF DIMENSION	0 HOURS	285 HOURS	500 HOURS	1000 HOURS	SAMPLE RANGE
	INCHES	INCHES	INCHES	INCHES	INCHES
XA	1.00069	1.00067	1.00066	1.00058	0.00011
XB	1.00008	1.00008	1.00008	1.00006	0.00002
XC	1.00053	1.00053	1.00052	1.00070	0.00018
XD	1.00046	1.00095	1.00093	1.00102	0.00056
XE	1.00040	1.00027	1.00042	1.00053	0.00026
YA	1.00046	1.00051	1.00039	1.00067	0.00028
YB	1.00128	1.00128	1.00126	1.00135	0.00009
YC	1.00087	1.00115	1.00093	1.00095	0.00028
YD	1.00032	1.00071	1.00032	1.00029	0.00042
YE	1.00122	1.00125	1.00117	1.00130	0.00013
ZC	0.69690	0.69687	0.69706	0.69698	0.00019
WEIGHT GRAMS	26.7431	26.7427	26.7426	26.7427	0.0005

BLOCK SERIAL NUMBER 9
TEST TEMPERATURE 1700 DEG-F

TOTAL TIME AT TEMPERATURE

FACE AND LOCATION OF DIMENSION	0 HOURS	285 HOURS	500 HOURS	1000 HOURS	SAMPLE RANGE
	INCHES	INCHES	INCHES	INCHES	INCHES
XA	1.00050	1.00042	1.00048	1.00048	0.00008
XB	1.00058	1.00053	1.00052	1.00051	0.00007
XC	1.00062	1.00047	1.00049	1.00064	0.00017
XD	1.00049	1.00038	1.00037	1.00033	0.00016
XE	1.00052	1.00041	1.00042	1.00037	0.00015
YA	1.00102	1.00086	1.00085	1.00095	0.00017
YB	1.00093	1.00086	1.00081	1.00080	0.00013
YC	1.00098	1.00096	1.00093	1.00104	0.00011
YD	1.00102	1.00091	1.00087	1.00093	0.00015
YE	1.00088	1.00084	1.00082	1.00086	0.00006
ZC	0.69686	0.69696	0.69688	0.69690	0.00010
WEIGHT GRAMS	26.7491	26.7458	26.7458	26.7457	0.0034

BLOCK SERIAL NUMBER 10
TEST TEMPERATURE 1700 DEG-F

TOTAL TIME AT TEMPERATURE

FACE AND LOCATION OF DIMENSION	0 HOURS	285 HOURS	500 HOURS	1000 HOURS	SAMPLE RANGE
	INCHES	INCHES	INCHES	INCHES	INCHES
XA	1.00076	1.00077	1.00073	1.00084	0.00011
XB	1.00080	1.00081	1.00074	1.00080	0.00007
XC	1.00084	1.00088	1.00088	1.00106	0.00022
XD	1.00093	1.00093	1.00093	1.00090	0.00003
XE	1.00091	1.00093	1.00087	1.00092	0.00006
YA	1.00095	1.00093	1.00096	1.00096	0.00003
YB	1.00105	1.00105	1.00104	1.00111	0.00007
YC	1.00098	1.00103	1.00106	1.00122	0.00024
YD	1.00102	1.00103	1.00097	1.00103	0.00006
YE	1.00117	1.00104	1.00112	1.00125	0.00021
ZC	0.69681	0.69681	0.69682	0.69682	0.00001
WEIGHT GRAMS	26.7581	26.7576	26.7575	26.7577	0.0006

BLOCK SERIAL NUMBER 11
TEST TEMPERATURE 1800 DEG-F

TOTAL TIME AT TEMPERATURE

FACE AND LOCATION OF DIMENSION	0 HOURS	285 HOURS	500 HOURS	1000 HOURS	SAMPLE RANGE
	INCHES	INCHES	INCHES	INCHES	INCHES
XA	1.00078	1.00118	1.00115	1.00116	0.00040
XB	1.00065	1.00116	1.00117	1.00117	0.00052
XC	1.00090	1.00117	1.00118	1.00118	0.00028
XD	1.00095	1.00117	1.00117	1.00118	0.00023
XE	1.00093	1.00115	1.00116	1.00113	0.00023
YA	1.00122	1.00077	1.00077	1.00074	0.00048
YB	1.00123	1.00090	1.00092	1.00094	0.00033
YC	1.00125	1.00087	1.00078	1.00080	0.00047
YD	1.00120	1.00060	1.00060	1.00059	0.00061
YE	1.00120	1.00072	1.00070	1.00072	0.00050
ZC	0.69691	0.69687	0.69692	0.69694	0.00007
WEIGHT GRAMS	26.7546	26.7541	26.7545	26.7544	0.0005

BLOCK SERIAL NUMBER 12
TEST TEMPERATURE 1800 DEG-F

TOTAL TIME AT TEMPERATURE

FACE AND LOCATION OF DIMENSION	0 HOURS	285 HOURS	500 HOURS	1000 HOURS	SAMPLE RANGE
	INCHES	INCHES	INCHES	INCHES	INCHES
XA	1.00128	1.00120	1.00122	1.00122	0.00008
XB	1.00125	1.00123	1.00119	1.00115	0.00010
XC	1.00123	1.00121	1.00117	1.00114	0.00009
XD	1.00114	1.00112	1.00107	1.00106	0.00008
XE	1.00113	1.00112	1.00107	1.00104	0.00009
YA	1.00105	1.00100	1.00096	1.00095	0.00010
YB	1.00098	1.00097	1.00093	1.00095	0.00005
YC	1.00099	1.00102	1.00093	1.00095	0.00009
YD	1.00098	1.00104	1.00096	1.00082	0.00022
YE	1.00083	1.00083	1.00081	1.00082	0.00002
ZC	0.69678	0.69677	0.69675	0.69675	0.00003
WEIGHT GRAMS	26.7428	26.7424	26.7425	26.7422	0.0006

BLOCK SERIAL NUMBER 13
TEST TEMPERATURE 1800 DEG-F

TOTAL TIME AT TEMPERATURE

FACE AND LOCATION OF DIMENSION	0 HOURS	285 HOURS	500 HOURS	1000 HOURS	SAMPLE RANGE
	INCHES	INCHES	INCHES	INCHES	INCHES
XA	1.00087	1.00087	1.00084	1.00092	0.00008
XB	1.00067	1.00062	1.00062	1.00055	0.00012
XC	1.00102	1.00098	1.00092	1.00101	0.00010
XD	1.00130	1.00117	1.00114	1.00115	0.00016
XE	1.00100	1.00097	1.00093	1.00095	0.00007
YA	1.00070	1.00067	1.00062	1.00066	0.00008
YB	1.00095	1.00082	1.00080	1.00088	0.00015
YC	1.00082	1.00073	1.00071	1.00082	0.00011
YD	1.00058	1.00054	1.00052	1.00050	0.00008
YE	1.00080	1.00074	1.00072	1.00069	0.00011
ZC	0.69677	0.69680	0.69676	0.69678	0.00004
WEIGHT GRAMS	26.7346	26.7345	26.7347	26.7345	0.0002

BLOCK SERIAL NUMBER 14
TEST TEMPERATURE 1800 DEG-F

TOTAL TIME AT TEMPERATURE

FACE AND LOCATION OF DIMENSION	0 HOURS	285 HOURS	500 HOURS	1000 HOURS	SAMPLE RANGE
	INCHES	INCHES	INCHES	INCHES	INCHES
XA	1.00013	1.00007	1.00012	1.00003	0.00010
XB	1.00072	1.00068	1.00067	1.00076	0.00009
XC	1.00042	1.00033	1.00036	1.00035	0.00009
XD	1.00008	1.00003	1.00004	0.99995	0.00013
XE	1.00063	1.00062	1.00059	1.00058	0.00005
YA	1.00082	1.00072	1.00080	1.00070	0.00012
YB	1.00004	1.00003	0.99996	0.99990	0.00014
YC	1.00057	1.00052	1.00062	1.00055	0.00010
YD	1.00111	1.00125	1.00110	1.00108	0.00017
YE	1.00032	1.00035	1.00027	1.00023	0.00012
ZC	0.69660	0.69662	0.69662	0.69664	0.00004
WEIGHT GRAMS	26.6866	26.6859	26.6862	26.6858	0.0008

BLOCK SERIAL NUMBER 15
TEST TEMPERATURE 1800 DEG-F

TOTAL TIME AT TEMPERATURE

FACE AND LOCATION OF DIMENSION	0 HOURS	285 HOURS	500 HOURS	1000 HOURS	SAMPLE RANGE
	INCHES	INCHES	INCHES	INCHES	INCHES
XA	1.00068	1.00066	1.00062	1.00065	0.00006
XB	1.00042	1.00033	1.00037	1.00085	0.00052
XC	1.00070	1.00056	1.00054	1.00085	0.00031
XD	1.00073	1.00066	1.00066	1.00079	0.00013
XE	1.00047	1.00041	1.00044	1.00053	0.00006
YA	1.00087	1.00087	1.00090	1.00087	0.00003
YB	1.00094	1.00092	1.00107	1.00090	0.00017
YC	1.00086	1.00086	1.00117	1.00097	0.00031
YD	1.00068	1.00065	1.00071	1.00080	0.00015
YE	1.00076	1.00072	1.00093	1.00076	0.00021
ZC	0.69652	0.69656	0.69653	0.69657	0.00005
WEIGHT GRAMS	26.7432	26.7430	26.7433	26.7430	0.0003

BLOCK SERIAL NUMBER 16
TEST TEMPERATURE 70 DEG-F

TOTAL TIME AT TEMPERATURE

FACE AND LOCATION OF DIMENSION	0 HOURS	285 HOURS	500 HOURS	1000 HOURS	SAMPLE RANGE
	INCHES	INCHES	INCHES	INCHES	INCHES
XA	1.00093	1.00091	1.00087	1.00085	0.00008
XB	1.00084	1.00084	1.00079	1.00085	0.00006
XC	1.00092	1.00092	1.00088	1.00083	0.00009
XD	1.00088	1.00092	1.00087	1.00084	0.00008
XE	1.00083	1.00083	1.00079	1.00080	0.00004
YA	1.00102	1.00113	1.00117	1.00108	0.00015
YB	1.00100	1.00095	1.00092	1.00100	0.00008
YC	1.00094	1.00093	1.00092	1.00093	0.00002
YD	1.00086	1.00088	1.00087	1.00083	0.00005
YE	1.00077	1.00075	1.00070	1.00073	0.00007
ZC	0.69678	0.69677	0.69670	0.69680	0.00010
WEIGHT GRAMS	26.7352	26.7353	26.7356	26.7354	0.0004

TABLE V

Experimental Design
Molding Experiment

Controlled Process Variables

Experiment Number	Die Temperature	Injection Pressure	Material Temperature	Hold Time
1	-	-	-	-
2	+	-	-	+
3	-	+	-	+
4	+	+	-	-
5	-	-	+	+
6	+	-	+	-
7	-	+	+	-
8	+	+	+	+

Experimental Responses

AFTER MOLDING

Density
Number of X-Ray Indications

AFTER BINDER REMOVAL

Number of Type 1 Cracks
Number of Type 2 Cracks
Number of Type 3 Cracks

TABLE VI

Direction of Movement of the Variables to Maximize Quality After Molding

	Die Temperature	Injection Pressure	Material Temperature	Hold Time
Maximize Density		↑	↓	
Minimize X-Ray Indications		↑	↓	

Note: Only effects significant at the 90% Confidence level are presented.

TABLE VII

Direction of Movement of the Variables to Maximize Quality After Binder Removal

	Die Temperature	Injection Pressure	Material Temperature	Hold Time
Minimize Type 1 Cracks	↓			↓
Minimize Type 2 Cracks	↓		↓	
Minimize Type 3 Cracks	↑	↓	↓	

Note: Only effects significant at the 90% confidence level are presented.

TABLE VIII

Experimental Design
Binder Removal Experiment

Experiment Number	Pressure	Heating Rate	Size (Complexity)
1	-	-	-
2	+	-	-
3	-	+	-
4	+	+	-
5	-	-	+
6	+	-	+
7	-	+	+
8	+	+	+

Responses

Percent Binder Removed
Number of Total Cracks

A = Pressure
B = Heating rate
C = Size (Complexity)

TABLE IX

Percent Binder Removal Results
2^3 Binder Removal Experiment

Effect	Magnitude
Total	
A	94.5
B	3.4
AB	0.4
C	0.9
AC	1.2
BC	0.6
ABC	0.1

To maximize percent binder removal: High Pressure
Large Size (Results confounded due to differences in material)

Pressure-Size interaction important

TABLE X

Percent Binder Removal Results
2^2 Binder Removal Experiment - Large Component Only

Effect	Magnitude
Total	94.75
A	2.15
B	-1.05
AB	0.65

To maximize percent binder removal: High Pressure
Low Rate

A = Pressure
B = Heating Rate
C = Size (Complexity)

TABLE XI

Total Crack Results
2^3 Binder Removal Experiment

Effect	Magnitude
Total	4.8
A	-7.3
B	0.1
AB	-2.1
C	9.6
AC	-7.3
BC	0.1
ABC	-2.1

To minimize cracking: Reduce Size, Complexity
Increase Pressure
Pressure-Size Interaction Important

TABLE XII

Crack Results
2^3 Binder Removal Experiment - Large Component Only

Effect	Magnitude
Total	6.1
A	-9.7
B	1.2
AB	1.2

To minimize cracking: Increase Pressure

TABLE XIII

Results of the Sintering-Strength Experiments

Condition	Dry Pressed			Injection Molded		
	Stress (Ksi)	m	Percent Density	Stress (Ksi)	m	Percent Density
1. Baseline (Long Time-High Temp.)	98	-	99	80-93	7-11	100
2. Short Time-High Temp.	103	15	99	-	-	-
3. Long Time-Low Temp.	94	7	97	-	-	-
4. Intermediate Time-Intermediate Temp.	133	22	100	75-88	8-12	100

m = Weibull modulus

TABLE XIV

Thermal Cycle Test

Time	Gage Reading Micro-inches			Temperature	Average Stress	Calculated Pressure
	1	2	3	°F	Psi	Psi
9:45	404	354	374	70	11310	1006
10:10	463	367	435	139	12660	1126
10:40	486	379	460	175	13230	1177
12:40	514	396	482	220	13920	1239
13:15	525	409	493	234	14250	1268
13:45	536	428	503	247	14670	1306
14:20	560	477	526	273	15630	1391
14:40	576	500	540	290	16160	1438
15:40	646	551	602	341	17990	1601
9:10	591	487	572	360	16500	1468
10:50	283	184	235	78	7020	624

TABLE XV

Publications Wholly or Partially Attributed to this Contract

1. Govila, R. K., "Methodology for Ceramic Life Prediction and Related Proof Testing," Tech. Rept. AMMRC TR 78-29, July, 1978.

2. Govila, R. K., "Ceramic Life Prediction Parameters," Tech. Rept. AMMRC TR 80-18, May, 1980.

3. Govila, R. K., "Indentation-Precracking and Double-Torsion Methods for Measuring Fracture Mechanics Parameters in Hot Pressed Silicon Nitride," Journal of The American Ceramic Society, Vol. 63, No. 5-6 May-June 1980.

4. Govila, R. K., "Uniaxial Tensile and Flexural Stress Rupture Strength of Hot-Pressed Silicon Nitride," Journal of The American Ceramic Society, Vol. 65. No. 1, January, 1982.

5. Baker, R. R., Swank, L. R., and Caverly, J. C., "Ceramic Life Prediction Methodology - Hot Spin Disc Life Program," Tech. Rept. AMMRC TR 82-26, April, 1982.

6. Swank, L. R., "Ceramic Life Prediction Methodology-Analytical Assessment of Selected Component Data," Tech. Rept. AMMRC TR 82-50, September 1982.

7. Govila, R. K., "High Temperature Strength Characterization of Sintered Alpha Silicon Carbide," Tech. Rept. AMMRC TR 82-51, October, 1982.

8. Govila, R. K., "Statistical Strength Evaluation of Hot-Pressed Silicon Nitride," Ceramic Bulletin, 62, [11], 1983.

9. Govila, R. K., High Temperature Uniaxial Tensile Stress Rupture Strength of Sintered Alpha SiC," Journal of Materials Science 18, 1967-1967, (1983).

10. Govila, R. K., "Material Parameters for Life Prediction," in Ceramics for High Performance Applications III, Editors Edward M. Lenoe, R. Nathan Katz, and John J. Burke, New York, Plenum Press, 1983.

11. Govila, R. K., "Flexural Stress Rupture Strength of Sintered Alpha Silicon Carbide," in Time-Dependent Failure Mechanisms and Assessment Methodologies, Editors J. G. Early, T. R. Shives, and J. H. Smith, New York, Cambridge University Press, 1983.

12. Baker, R. R., Swank, L. R., and Caverly, J. C., "Ceramic Life Prediction Methodology - Hot Spin Disc Life Program," Tech. Rept. AMMRC TR 83-44, August, 1983.

13. Swank, L. R., Baker, R. R., and Lenoe, E. M., "Ceramic Life Prediction Methodology", Proceedings of the Twenty-First Automotive Technology Development Contractors Coordination Meeting, SAE P-138, November, 1983.

14. Covila, R. K., Phenomenology of Fracture in Sintered Alpha Silicon Carbide", Journal of Materials Science 19, 2111-2120 (1984).

15. Govila, R. K., "Strength Characterization and Nature of Crack Propagation in Sintered Alpha Silicon Carbide," Proceedings: Sixth International Conference on Fracture, Editors S. R. Valluvi, P. Rama Rao, and K. N. Raju, Cambridge, England, Pergammon Press, 1984.

TABLE XVI

Patents Wholly or Partially Attributed to this Contract

Method of Attaching a Metal Shaft to a Ceramic Shaft and Product Produced Thereby, U. S. Patent 4,485,545.

Method of Attaching a Metal Shaft to a Ceramic Shaft and Product Produced Thereby, U. S. Patent 4,499,646.

REFERENCES

1. Govila, R. K., "Methodology for Ceramic Life Prediction and Related Proof Testing," Tech. Rept. AMMRC TR 78-29, July, 1978.

2. Govila, R. K., "Ceramic Life Prediction Parameters," Tech. Rept. AMMRC TR 80-18, May, 1980.

3. Govila, R. K., "Indentation-Precracking and Double-Torsion Methods for Measuring Fracture Mechanics Parameters in Hot-Pressed Silicon Nitride," Journal of The American Ceramic Society, Vol. 63, No. 5-6 May-June 1980.

4. Govila, R. K., "Uniaxial Tensile and Flexural Stress Rupture Strength of Hot-Pressed Silicon Nitride," Journal of The American Ceramic Society, Vol. 65. No. 1, January, 1982.

5. Govila, R. K., "Statistical Strength Evaluation of Hot-Pressed Silicon Nitride," Ceramic Bulletin, 62, [11], 1983.

6. Govila, R. K., "High Temperature Strength Characterization of Sintered Alpha Silicon Carbide," Tech. Rept. AMMRC TR 82-51, October, 1982.

7. Govila, R. K., High Temperature Uniaxial Tensile Stress Rupture Strength of Sintered Alpha SiC," Journal of Materials Science 18, 1967-1976, (1983).

8. Govila, R. K., Phenomenology of Fracture in Sintered Alpha Silicon Carbide", Journal of Materials Science 19, 2111-2120 (1984).

9. Swank, L. R., "Ceramic Life Prediction Methodology-Analytical Assessment of Selected Component Data," Tech. Rept. AMMRC TR 82-50, September 1982.

10. Baker, R. R., Swank, L. R., and Caverly, J. C., "Ceramic Life Prediction Methodology - Hot Spin Disc Life Program," Tech. Rept. AMMRC TR 82-26, April, 1982.

11. Baker, R. R., Swank, L. R., and Caverly, J. C., "Ceramic Life Prediction Methodology - Hot Spin Disc Life Program," Tech. Rept. AMMRC TR 83-44, August, 1983.

12. Govila, R. K., Herman J. A., and Arnon, N., "Stress Rupture Test Rig Design for Evaluating Ceramic Material Specimens," ASME Paper #85-GT-181, March 18, 1985.

13. Govila, R. K., Kinsman, K. R., and Beardmore, P., "Fracture Phenomenology of a Lithium-Aluminium-Silicate Glass-Ceramic," Journal of Material Science, 13 [4] 2081-2091 (1978).

14. Lipson, C., and Sheth, N. J., Statistical Design and Analysis of Engineering Experiments, New York, McGraw-Hill, 1973.

DISTRIBUTION LIST

Donald F. Adams
Composite Materials Research Group
Mechanical Engineering Department
University of Wyoming
Laramie, WY 82071

Jane W. Adams
Corning Glass Works
SP-DV-21
Corning, NY 14831

Anil K. Agarwal
Product Manager
High Performance Ceramics
Norton Company
One New Bond Street
Worcester, MA 01606

Richard T. Alpaugh
Department of Energy
Office of Transportation Systems
CE-131 FORSTL
1000 Independence Avenue
Washington, DC 20585

James P. Arnold
U.S. Army Belvoir
R&D Center
ATTN: FTRBE-EMP
Fort Belvoir, VA 22060

V. S. Avva
Dept. of Mechanical Engineering
North Carolina Agricultural and
Technical State University
Greensboro, NC 27411

John M. Bailey
Research Consultant, Research Dept.
Technical Center
Caterpillar Tractor Co.
100 NE Adams
Peoria, IL 61629

Murray Bailey
NASA Lewis Research Center
21000 Brookpark Road, MS 77-6
Cleveland, OH 44135

J. Gary Baldoni
GTE Laboratories, Inc.
40 Sylvan Road
Waltham, MA 02254

R. R. Baker
34819 Lyndon Street
Livonia, MI 48154

Ken Baumert
Air Products and Chemicals, Inc.
Box 538
Allentown, PA 18105

Ronald L. Beatty
ARCO Chemicals, Silag Operation
Route 6, Box A
Greer, SC 29651

A. L. Bement, Jr., Vice President
Technical Resources
TRW, Inc.
23555 Euclid Avenue
Cleveland, OH 44117

Clifton G. Bergeron, Head
Department of Ceramic Engineering
204 Ceramics Building
University of Illinois
Urbana, IL 61801

William D. Bjorndahl
TRW, Inc.
TRW Energy Development Group
Materials Characterization and
Chemical Analysis Dept.
One Space Park
Building 01, Room 2060
Redondo Beach, CA 90278

Paul N. Blumberg
President
Integral Technologies Inc.
415 E. Plaza Drive
Westmont, IL 60559

Wolfgang D. G. Boecker
SOHIO Engineered Materials Co.
Niagara Falls R&D Center
PO Box 832
Niagara Falls, NY 14302

Seymour A. Bortz
Manager, Nonmetallic Materials
and Composites
Materials and Manufacturing
Technology
IIT Research Institute
10 West 35th Street
Chicago, IL 60616

H. K. Bowen
Department of Materials Science
and Engineering, Room 12-009
Massachusetts Institute of
Technology
Cambridge, MA 02139

Richard C. Bradt
University of Washington
Roberts Hall
FB-10
Seattle, WA 98195

Raymond J. Bratton
Manager, Ceramic Science
Westinghouse Research and
Development Center
1310 Beulah Road
Pittsburgh, PA 15235

W. Bryzik
US Army Tank Automotive Command
(TACOM)
R&D Center
Warren, MI 48090

S. T. Buljan
GTE Laboratories, Inc.
40 Sylvan Road
Waltham, MA 02154

John M. Byrne, Jr.
Manager, Business Development
Corporate Development Department
PPG Industries, Inc.
One PPG Place
Pittsburgh, PA 15272

Donald J. Campbell
Air Force Wright Aeronautical
Laboratory
AFWAL/POX
Wright-Patterson AFB, OH 45433

Harry W. Carpenter
Rockwell International
Rocketdyne Division
J39-169:HC92
6633 Canoga Avenue
Canoga Park, CA 91304

David Carruthers
Garrett Turbine Engine Company
111 South 34 Street
PO Box 5217
Phoenix, AZ 85010

Se-Tak Chang
GTE Laboratories
40 Sylvan Road
Dept. 312
Waltham, MA 02254

En-sheng Chen
B&C Engineering Research
13906 Dentwood Drive
Houston, TX 77014

Albert A. Chesnes
Director
Heat Engine Propulsion Division
Office of Transportation Systems
Department of Energy
CE-131 FORSTL
1000 Independence Avenue
Washington, DC 20585

Melvin H. Chiogioji
Director
Office of Transportation Systems
Department of Energy
CE-13 FORSTL
1000 Independence Avenue, SW
Washington, DC 20585

William J. Chmura
The Torrington Company
Corporate Research
59 Field Street
Torrington, CT 06790

William L. Cleary
Associate Division Director
ORI, Inc.
1375 Piccard Drive
Rockville, MD 20850

Philip R. Compton
Energy Systems Office
National Aeronautics and
Space Administration
Code REC-1
Washington, DC 20546

John A. Coppola
Representative Director
Executive Vice President
Hitachi-Carborundum Company
Shinjuku-Mitsui Building
No. 1-1, 2-Chome, Nishishinjuku
Shinjuku-ku, Tokyo 160, JAPAN

C. H. Craig
Department of Energy
1000 Independence Avenue
CE-131 FORSTL
Washington, DC 20585

William J. Croft
U. S. Army Materials Technology Laboratory (MTL)
Arsenal Street
Watertown, MA 02172

Gary M. Crosbie
Ford Motor Company
PO Box 2053, Room S-2079
Ceramics Materials Department
Dearborn, MI 48121

Floyd W. Crouse, Jr.
Department of Energy
Morgantown Energy Technology Center
PO Box 880
Morgantown, WV 26505

Raymond Cutler
Ceramatec, Inc.
163 West 1700 South
Salt Lake City, UT 84115

Stanley J. Dapkunas
Office of Technical Coordination
Fossil Energy Technical
Coordination Staff
FE-14, MS B127 GTN
Department of Energy
Washington, DC 20545

Robert F. Davis
North Carolina State University
Materials Engineering Department
232 Riddick Laboratory
Raleigh, NC 27607

Alan L. Dragoo
Materials Scientist, Inorganic
Materials Division
National Bureau of Standards
Center for Materials Science
Gaithersburg, MD 20899

Keith F. Dufrane
Battelle Columbus Laboratories
505 King Avenue
Columbus, OH 43201

Robert J. Eagan
Manager, Chemistry and Ceramics
Department 1840
Sandia National Laboratories
Albuquerque, NM 87185

Christopher A. Ebel
Program Manager
Norton Company
High Performance Ceramics
1 New Bond Street
Worchester, MA 01606

J. J. Eberhardt
Office of Energy Utilization
Research
Department of Energy
CE-142 FORSTL
1000 Independence Avenue
Washington, DC 20585

E. E. Ecklund
Office of Transportation Systems
Department of Energy
CE-131 FORSTL
1000 Independence Avenue
Washington, DC 20585

William A. Ellingson
Argonne National Laboratory
9700 South Cass Avenue
Argonne, IL 60439

Director, Applied Technology
Laboratory
U.S. Army Research and Technology
Laboratory (AVSCOM)
ATTN: SAVDL-ATL-ATP
(Graydon A. Elliott)
Fort Eustis, VA 23604

A. Erdely
Chemical Engineer
26 Avenue Gare Des Eaux-vives
1208 Geneva, SWITZERLAND

Charles D. Estes
U.S. Senate
Professional Staff Member
Committee on Appropriations
Room SD-152 Dirksen Senate
Office Building
Washington, DC 20510

Anthony G. Evans
University of California
Santa Barbara, CA 93106

Robert C. Evans, Asst. Manager
Vehicular Gas Turbine and Diesel
Project Office
NASA-Lewis Research Center
21000 Brookpark Road
Cleveland, OH 44135

John Facey
National Aeronautics and
Space Administration
Energy Systems Office
Washington, DC 20546

John W. Fairbanks
Office of Advanced Energy
Conversion
Department of Energy
FE-22 GTN
Washington, DC 20545

Larry Farrell
Babcock and Wilcox
PO Box 1260
Lynchburg, VA 24505

Matthew K. Ferber
University of Illinois-Urbana
203 Ceramic Building
105 S. Goodwin Avenue
Urbana, IL 61801

R. E. Fisher
President
Amercom, Inc.
8948 Fullbright Avenue
Chatsworth, CA 91311

H. W. Foglesong
Dow Corning Corporation
3901 S. Saginaw Road
Midland, MI 48640

Robert G. Frank
Manager, Non-Metallic Materials
General Electric Company
One Neumann Way, Mail Drop M-87
PO Box 156301
Cincinnati, OH 45215-6301

Frank Gac
Department of Materials Science
and Engineering
University of Washington
Seattle, WA 98195

George E. Gazza
Materials Technology Laboratory
Ceramics Research Division
AMXMR-MT
Arsenal Street
Watertown, MA 02172

Paul Glance
Director, R&D
Concept Analysis Corporation
9145 General Court
Plymouth, MI 48170

Joseph W. Glatz
Naval Air Propulsion Center
Science and Technology Group
Systems Technology Division
Box 7176, PE 34
Trenton, NJ 08628

S. Goguen
Office of Transportation Systems
Department of Energy
CE-131 FORSTL
1000 Independence Avenue
Washington, DC 20585

Stephen T. Gonczy
Allied Signal Research Center
Materials Science Department
50 UOP Plaza
Des Plaines, IL 60016-6187

Robert J. Gottschall
Office of Material Sciences
Department of Energy
ER-131 GTN
Washington, DC 20545

Kenneth Green
Senior Development Engineer
Coors Porcelain Company
Golden, CO 80401

Michael Greenfield
National Aeronautics and
Space Administration
Energy Systems Office
Washington, DC 20546

L. E. Groseclose
General Motors Corporation
Allison Gas Turbine Division
P.O. Box 420
Indianapolis, IN 46206-0420

T. D. Gulden, Manager
Ceramics and Chemistry
GA Technologies, Inc.
PO Box 81608
San Diego, CA 92138

M. D. Gurney
NIPER
PO Box 2128
Bartlesville, OK 74005

H. T. Hahn
Mechanical Engineering Department
Washington University
at St. Louis
Lindell and Skinker
Box 1087
St. Louis, MO 63130

Nabil S. Hakim
Staff Research Engineer
Engineering R&D
General Motors Corporation
Detroit Diesel Allison Division
36880 Ecorse Road
Romulus, MI 48174

John M. Halstead
Manager, Business Development
Structural Ceramics Division
Standard Oil Engineered Materials Company
1625 Buffalo Avenue, Bldg. 91-2
PO Box 1054
Niagara Falls, NY 14302

R. A. Harmon
25 Schalren Drive
Latham, NY 12110

Stephen D. Hartline
Norton Company
One New Bond Street
Worchester, MA 01606

Willard E. Hauth
Section Manager - Composite
Development Ceramics Program
Dow Corning Corporation
Midland MI 48640

Norman L. Hecht
University of Dayton Research
Institute
300 College Park
Dayton, OH 45469-0001

S. S. Hecker, Chairman
Center for Materials Science
Los Alamos National Laboratory
Mail Stop K765
Los Alamos, NM 87545

Peter W. Heitman
General Motors Corporation
Allison Gas Turbine Operations
PO Box 420, W-5
Indianapolis, IN 46206-0420

H. E. Helms
General Motors Corporation
Allison Gas Turbine Operations
PO Box 420
Indianapolis, IN 46206-0420

Thomas L. Henson, Director of
Research and Engineering
Chemical & Metallurgical Division
GTE Products Corporation
Hawes Street
Towanda, PA 18848-0504

Thomas P. Herbell
NASA Lewis Research Center
21000 Brookpark Road
M/S 49-3
Cleveland, OH 44135

Robert V. Hillery, Manager
Coating Materials & Processes
General Electric Company
Cincinnati, OH 45215

Jonathan W. Hinton
Vice President and General Manager
Structural Ceramics Division
SOHIO Engineered Materials Company
PO Box 1054
Niagara Falls, NY 14302

Stephen M. Hsu
Inorganic Materials Div.
Center for Materials Science
U.S. Department of Commerce
National Bureau of Standards
Gaithersburg, MD 20899

Harold A. Huckins, President
Princeton Advanced Technology, Inc.
56 Finley Road
Princeton, NJ 08540

Joseph E. Hunter, Jr.
Metallurgy Department
General Motors Research Lab.
12 Mile and Mound Road
Warren, MI 48090-9055

Louis C. Ianniello, Director
Office of Materials Sciences
Department of Energy
ER-13 GTN
Washington, DC 20545

Curtis A. Johnson
General Electric Company
Ceramics Branch
PO Box 8
Schenectady, NY 12301

Larry Johnson, Director
Center for Transportation Resear
Argonne National Laboratory
Building 362
9700 S. Cass Avenue
Argonne, IL 60439

R. A. Johnson
General Motors Corporation
Allison Gas Turbine Division
P.O. Box 420
Indianapolis, IN 46206-0420

L. A. Joo
Associate Director of Research
Great Lakes Research Corp.
P.O. Box 1031
Elizabethton, TN 37643

Roy Kamo, President
Adiabatics, Inc.
630 S. Mapleton
Columbus, IN 47201

Allan Katz
Air Force Wright Aeronautical
Laboratory
Materials Laboratory
Metals and Ceramics Division
AFWAL/MLLM
Wright-Patterson AFB, OH 45433

R. N. Katz
Chief, Ceramics Research Division
DRXMR-MC
U. S. Army Materials Technology Laboratory
Arsenal Street
Watertown, MA 02172

P. Victor Kelsey
Ceramics Technical Leader
Materials Science Division
Alcoa Aluminum Company
of America
Alcoa Technical Center B
Alcoa Center, PA 15061

Frederick L. Kennard, III
Supervisor, Ceramic Research
AC Spark Plug Division of
General Motors
1300 N. Dort Highway
Flint, MI 48556

J. R. Kidwell
AGT 101 Assistant Project Engineer
Garrett Turbine Engine Company
111 S. 34th Street
P.O. Box 5217
Phoenix, AZ 85010

A. S. Kobayashi
Mechanical Engineering Dept.
MS FU10
University of Washington
Seattle, WA 98195

David M. Kotchick
AiResearch Manufacturing Company
2525 W. 190th Street
Torrance, CA 90509

Saunders B. Kramer
Manager, AGT Program
Office of Transportation Systems
Department of Energy
CE-131 FORSTL
1000 Independence Avenue
Washington, DC 20585

D. M. Kreiner
AGT 101 Project Manager
Garrett Turbine Engine Company
111 S. 34th Street
P.O. Box 5217
Phoenix, AZ 85010

W. J. Lackey
Georgia Tech Research Institute
Energy and Materials Sciences Laboratory
Georgia Institute of Technology
Atlanta, GA 30332

Everett A. Lake
Air Force Wright Aeronautical
Laboratory
AFWAL/POOS
Wright-Patterson AFB, OH 45433

Fred F. Lange
Science Center
Rockwell International
1049 Camino Dos Rios
PO Box 1085
Thousand Oaks, CA 91360

John G. Lanning
Corning Glass Works
Advanced Engine Components
HP-BB-2
Corning, NY 14830

David C. Larsen
IIT Research Center
10 W. 35th Street
Chicago, IL 60616

E. M. Lenoe
U. S. Army Materials Technology Laboratory
DRXMR-MC
Arsenal Street
Watertown, MA 02172

Stanley R. Levine
NASA-Lewis Research Center
21000 Brookpark Road
Cleveland, OH 44135

David Lewis
Naval Research Laboratory
Code 6360, Materials Science &
Technology Division
4555 Overlook Avenue, S.W.
Washington, DC 20375

Winston W. Liang
Project Manager
Industrial Materials Research
Gas Research Institute
8600 W. Bryn Mawr Avenue
Chicago, IL 60631

Bill Long
Elektroschmetlzwerk Kempten GmbH
Post Office Box 590
Tonawanda, N. Y. 14151-0590

L. A. Lott
EG&G, Inc.
Idaho National Engineering
Laboratory
PO Box 1625
Idaho Falls, ID 83415

Bryan K. Luftglass
Staff Consultant
Chem Systems, Inc.
303 S. Broadway
Tarrytown, NY 10591

Michael J. Lynch
General Electric Company
Medical Systems Group
PO Box 414, 7B-36
Milwaukee, WI 53201

Tai-il Mah
Technical Manager
Ceramics and Composites Research
Universal Energy Systems
4401 Dayton-Xenia Road
Dayton, OH 45432

John Mason
Vice President-Engineering
The Garrett Corporation
9851 Sepulveda Boulevard
PO Box 92248
Los Angeles, CA 90009

K. S. Mazdiyasni
Air Force Wright Aeronautical
Laboratory
Materials Laboratory
Metals and Ceramics Division
AFWAL/MLLM
Wright-Patterson AFB, OH 45433

J. McCauley
U. S. Army Materials Technology Laboratory
DRXMR-MC
Department of the Army
Arsenal Street
Watertown, MA 02171

Thomas D. McGee
Department of Materials Science
and Engineering
Iowa State University
Ames, IA 50011

Malcolm G. McLaren
Head, Department of Ceramics
Rutgers University
Busch Campus
Box 909, Bowser Road
Piscataway, NJ 08854

Arthur F. McLean
Ceramics Materials Department
Ford Motor Company
PO Box 2053
Dearborn, MI 48121

Brian L. Mehosky
Development Engineer, R&D
Standard Oil Engineered Materials Company
4440 Warrensville Center Road
Cleveland, OH 44128

P. K. Mehrotra
Kennametal Inc.
P.O. Box 639
Greensburg, PA 15601

Donald Messier
Army Materials Technology Laboratory
DRXMR-MC
Department of the Army
Arsenal Street
Watertown, MA 02171

Arthur G. Metcalfe
Director, Research Department
Solar Turbines, Inc.
PO Box 80966
2200 Pacific Highway
San Diego, CA 92138

Thomas N. Meyer
Senior Technical Specialist
Alumina, Chemicals and Ceramics Div.
Aluminum Company of America
Alcoa Technical Center
Alcoa Center, PA 15069

W. Miloscia
Standard Oil Engineered Materials Company
Research and Development
4440 Warrensville Center Road
Cleveland, OH 44128

Helen Moeller
Babcock & Wilcox
P.O. Box 1260
Lynchburg, VA 24505

Peter E. D. Morgan
Member Technical Staff
Structural Ceramics
Science Center
Rockwell International
1049 Camino Dos Rios
PO Box 1085
Thousand Oaks, CA 91360

James I. Mueller
Ceramic Engineering Dept.
MS FB10
University of Washington
Seattle, WA 98195

Solomon Musikant
General Electric, VFSC
Building 100, U-3027
PO Box 8555
Philadelphia, PA 19101

Dale E. Niesz
Manager, Materials Department
Battelle Columbus Laboratories
505 King Avenue
Columbus, OH 43201

W. Richard Ott
New York State College of Ceramics
Alfred University
Alfred, NY 14802

Hayne Palmour III
Engineering Research Services
Division
2158 Burlington Engineering
Laboratories
North Carolina State University
PO Box 5995
Raleigh, NC 27607

Joseph N. Panzarino
Norton Company
Director, Research and Development
High Performance Ceramics
1 New Bond Street
Worcester, MA 01606

Pellegrino Papa, Manager
Technical and Business Development
Corning Technical Products Division
Corning Glass Works
Corning, NY 14831

Arvid E. Pasto
Member of Technical Staff
Precision Materials Technology
GTE Laboratories, Inc.
40 Sylvan Road
Waltham, MA 02254

James W. Patten
Director, Materials Engineering
Cummins Engine Company, Inc.
Mail Code 50183
Box 3005
Columbus, IN 47201

Dan Petrak
Babcock and Wilcox
PO Box 1260
Lynchburg, VA 24505

R. Byron Pipes
Center for Composite Materials
2001 Spencer Laboratory
University of Delaware
Newark, DE 19716

Robert C. Pohanka
Office of Naval Research
Code 431
800 North Quincy Street
Arlington, VA 22217

Karl M. Prewo
United Technologies Research Center
Silver Lane, MS 24
East Hartford, CT 06108

Hubert B. Probst
Chief Scientist
Materials Division, MS 49-1
NASA-Lewis Research Center
21000 Brookpark Road
Cleveland, OH 44135

Carr Lane Quackenbush
GTE Products Corporation
Hawes Street
Towanda, PA 18848-0504

George Quinn
Army Materials Technology Laboratory
Ceramic Research Division
AMXMR-MV
Arsenal Street
Watertown, MA 02172

Dennis T. Quinto
Phillip M. McKenna Laboratory
Kennametal, Incorporated
Post Office Box 639
Greensburg, PA 15601

Dennis Readey
Department Chairman
Ceramic Engineering Department
Ohio State University
2041 College Road
Columbus, OH 43210

Robert R. Reeber
U.S. Army Research Office
PO Box 12211
Research Triangle Park, NC 27709

K. L. Reifsnider
Department of Engineering Scienc
and Mechanics
Virginia Polytechnic Institute
and State University
Blacksburg, VA 24061

K. T. Rhee
College of Engineering
Rutgers University
P.O. Box 909
Piscataway, NJ 08854

Roy W. Rice
W. R. Grace and Company
7379 Route 32
Columbus, MD 21044

David W. Richerson
Ceramatec, Inc.
163 West 1700 South
Salt Lake City, UT 84115

Paul Rieth
Ferro Corporation
661 Willet Road
Buffalo, NY 14218

Michael A. Rigdon
Babcock and Wilcox
1735 I Street, NW
Washington, DC 20006

John E. Ritter, Jr.
University of Massachusetts
Mechanical Engineering Department
Amherst, MA 01003

Giulio A. Rossi
Norton Company
High Performance Ceramics
Goddard Road
Northboro, MA 01532

Barry R. Rossing
Aluminum Company of America
Alcoa Technical Center
Alcoa Center, PA 15069

David J. Rowcliffe
SRI International
333 Ravenswood Avenue
Menlo Park, CA 94025

Donald W. Roy, Manager
Carbide and Optical Material
Research and Development
Coors Porcelain Company
Golden, CO 80401

Bruce Rubinger
Gobal
50 Milk Street
15th Floor
Boston, MA 02109

Robert Ruh
Air Force Wright Aeronautical
Laboratory
Materials Laboratory
Metals and Ceramics Division
AFWAL/MLLM
Wright-Patterson AFB, OH 45433

Robert J. Russell, Sr.
Divisional Vice President
Technology and Planning
High Performance Ceramics
Norton Company
One New Bond Street
Worchester, MA 01606

J. Sankar
North Carolina Agricultural
and Technical State University
Mechanical Engineering Dept.
Greenboro, NC 27411

Maxine Savitz
5019 Lowell Street, NW
Washington, DC 20016

Richard Schapery
Civil Engineering Department
Texas A&M University
College Station, TX 77843

Liselotte J. Schioler
Army Materials Technology Laboratory
Ceramic Research Div.
AMXMR-MC
Arsenal Street
Watertown, MA 02172

Matthew Schreiner
Gas Research Institute
8600 West Bryn Mawr Avenue
Chicago, IL 60631

Peter C. Schultz
Manager, Materials Research
Corning Research and Development
Division
Corning Glass Works
Corning, NY 14831

R. B. Schulz
Office of Transportation Systems
Department of Energy
CE-131 FORSTL
1000 Independence Avenue
Washington, DC 20585

Murray A. Schwartz
Bureau of Mines
2401 I Street, N.W.
Washington, DC 20241

Thomas M. Sebestyen
U.S. Army Tank Automotive Comman
AMSTA-RGRT
Warren, MI 48397-5000

Brian Seegmiller
Senior Development Engineer
Coors Porcelain Company
17750 North 32 Street
Golden, CO 80401

S. G. Seshadri
Research Associate
Standard Oil Engineered Materials Company
Niagara Falls R&D Center
PO Box 832
Niagara Falls, NY 14302

Peter T. B. Shaffer
Executive Vice President
Advanced Refractory
Technologies, Inc.
699 Hertel Avenue
Buffalo, NY 14207

Dinesh K. Shetty
The University of Utah
Dept. of Materials Science & Engrg.
Salt Lake City, UT 84112

Jack D. Sibold
Coors Porcelain Company
17750 North 32 Street
Golden, CO 80401

Neal Sigmon
Appropriations Committee
Subcommittee on Interior and
Related Events
U.S. House of Representatives
B-308 Rayburn Building
Washington, DC 20515

Richard Silberglitt
DHR, Inc.
6849 Old Dominion Drive
Suite 228
McLean, VA 22101

S. R. Skaggs
MS F-682, Program Office
Los Alamos National Laboratory
PO Box 1663
Los Alamos, NM 87545

Ed Skorupski
Air Products and Chemicals, Inc.
PO Box 538
Allentown, PA 18105

J. Thomas Smith, Director
Precision Materials Tech.
GTE Laboratories, Inc.
40 Sylvan Road
Waltham, MA 02254

Jay R. Smith
Senior Development Specialist
Garrett Turbine Engine Company
2739 E. Washington, MS 93-172/1302-2K
Phoenix, AZ 85034

Rafal Sobotowski
Standard Oil Engineered Materials Company
Research and Development
3092 Broadway Avenue
Cleveland, OH 44115

Richard M. Spriggs
National Materials Advisory Board
National Research Council
2101 Constitution Avenue
Washington, DC 20418

M. Srinivasan
Standard Oil Engineered Materials Company
Niagara Falls R&D Center
PO Box 832)
Niagara Falls, NY 14302

Gordon L. Starr, Manager
Metallic/Ceramic Materials Dept.
Cummins Engine Company, Inc.
Mail Code 50183
Box 3005
Columbus, IN 47202-3005

Harold L. Stocker, Manager
Low Heat Rejection Program
General Motors Corporation
Allison Gas Turbine Operations
PO Box 420, T-23
Indianapolis, IN 46206-0420

Roger Storm
Director, Niagara Falls R&D Center
Standard Oil Engineered Materials Company
PO Box 832
Niagara Falls, NY 14302

E. E. Strain
Program Manager
Garrett Turbine Engine Company
111 S. 34th Street
PO Box 5217, Mail Stop 301-2N
Phoenix, AZ 85010

Thomas N. Strom
NASA Lewis Research Center
21000 Brookpark Road, 77-6
Cleveland, OH 44135

Karsten Styhr
AiResearch Casting Co.
19800 Van Ness Avenue
Torrance, CA 90509

Lewis R. Swank
Ford Motor Company
PO Box 2053
Building SRL, Room E3172
Dearborn, MI 48121

Anthony C. Taylor
Staff Director
Subcommittee on Transportation,
Aviation and Materials
Committee on Science and
Technology
U.S. House of Representatives
Room 2321 Rayburn Building
Washington, DC 20515

W. H. Thielbahr
Chief, Energy Programs Branch
Idaho Operations Office
U.S. Department of Energy
550 2nd Street
Idaho Falls, ID 83401

John K. Tien
Director of Center for
Strategic Materials
1137 S.W. Mudd Building
Columbia University
New York, NY 10027

T. Y. Tien
University of Michigan
Dept. of Materials &
Metallurgical Engineering
Dow Building
Ann Arbor, MI 48109-2136

Nancy J. Tighe
National Bureau of Standards
Inorganic Materials Division 420
Gaithersburg, MD 20899

Julian M. Tishkoff
Air Force Office of
Scientific Research
Directorate of Aerospace Sciences
Bolling AFB
Washington, DC 20332

Maurice L. Torti
Senior Scientist
High Performance Ceramics
Norton Company
One New Bond Street
Worchester, MA 01606

Louis E. Toth
Division of Materials Research
National Science Foundation
1800 G Street, N.W.
Washington, DC 20550

Richard E. Tressler
Chairman, Ceramic Science and
Engineering Department
The Pennsylvania State University
201 Steidle Building
University Park, PA 16802

V. Venkateswaran
Standard Oil Engineered Materials Company
PO Box 832
Niagara Falls, NY 14302

John B. Wachtman, Jr.
Rutgers University
Department of Ceramics
PO Box 901
Piscataway, NJ 08854

Richard B. Wallace
Manager, Government Research
and Development Programs
General Motors Corporation
Detroit Diesel Allison Division
36880 Ecorse Road
Romulus, MI 48174

Harlan L. Watson
Subcommittee on Energy Research
and Production
U.S. House of Representatives
Committee on Science and
Technology
Suite 2321, Rayburn House
Office Building
Washington, DC 20515

Steven G. Wax
Materials Science Division
Advanced Research Projects Agency
Department of Defense
1400 Wilson Boulevard
Arlington, VA 22209

Albert R. C. Westwood
Corporate Director
Martin Marietta Laboratories
1450 South Rolling Road
Baltimore, MD 21227

Thomas J. Whalen
Principal Research Scientist
Ford Motor Company
Scientific Lab, Room 2023
Dearborn, MI 48121

Sheldon M. Wiederhorn
Inorganic Materials Division
Mechanical Properties Group
U.S. Department of Commerce
National Bureau of Standards
Gaithersburg, MD 20899

James C. Williams
Dean
Carnegie Institute of Technology
Carnegie-Mellon University
Schenley Park
Pittsburgh, PA 15213

Roger R. Wills, Manager
Advanced Ceramic Components
TRW Inc.
Automotive Worldwide Sector
Valve Division
1455 East 185th Street
Cleveland, OH 44110

David Gordon Wilson
Massachusetts Institute of
Technology
Mechanical Engineering Department
Room 3-455
Cambridge, MA 02139

J. M. Wimmer, Supervisor
Nonmetallic Materials Group
Garrett Turbine Engine Company
111 S. 34th Street
P.O. Box 5217
Phoenix, AZ 85010

David Wirth, Vice President
Technical Operations and Engr.
Coors Porcelain Company
17750 North 32 Street
Golden, CO 80401

Thomas J. Wissing
Manager, Government
Contract Administration
Eaton Corporation
Engineering & Research Center
26201 Northwestern Highway
PO Box 766
Southfield, MI 48037

James C. Wood
NASA Lewis Research Center
21000 Brookpark Road
Mail Stop 77-6
Cleveland, OH 44135

Hun C. Yeh
Ceramic Supervisor
AiResearch Casting Company
A Division of the Garrett Corp.
19800 Van Ness Avenue
Torrance, CA 90509

Thomas M. Yonushonis
Cummins Engine Company
Box 3005, Mail Code 50183
Columbus, IN 47202-3005

Don Zabierek
Air Force Wright Aeronautical
Laboratory
AFWAL/POTC
Wright-Patterson AFB, OH 45433

Klaus M. Zwilsky
Executive Director
National Materials Advisory Board
National Research Council
2101 Constitution Avenue
Washington, DC 20418

Department of Energy
Oak Ridge Operations Office
Office of Assistant Manager for
Energy Research and Development
PO Box E
Oak Ridge, TN 37831

Department of Energy
Technical Information Center
Office of Information Services
PO Box 62
Oak Ridge, TN 37831

U S Army Materials Technology Laboratory
Watertown, Massachusetts 02172-0001
Ceramic Life Prediction
Methodology-Final Report
L R Swank, J A Mangels, J C Conway
and R E Gentile
Research Staff
Ford Motor Company
P O Box 2053
Dearborn, Michigan 48121
Technical Report MTL TR 86-14, May 1986, 43pp.
Illus.-tables, Contract DAAG46-77-C-0078
DOE I No DE-AI03-84GE71411
Final Report January 1983 to December 1985

AD_____
UNCLASSIFIED
UNLIMITED DISTRIBUTION

Key Words

Ceramic materials
Life expectancy
Disks
Test and evaluation
Silicon nitride
Glass ceramics
Gas turbine
Brittle materials design

Fast fracture and stress rupture data were collected on two materials, a sintered silicon nitride and a lithium-aluminum-silicate. The fast fracture data was presented graphically in the form of Weibull plots of percent failed versus failure stress. The stress rupture results were presented in tabular form. Photo-micrographs were presented to illustrate the fracture surfaces of fast fracture and stress rupture failures. A program of specimen development was conducted. The objective of the program was to develop processing techniques to make it possible to fabricate integral shaft spin disks suitable for hot spin testing as stress rupture specimens. The hot spin disk stress rupture results were to be used to correlate experimental time dependent failure results with analytical time dependent failure results. In the specimen development program several sets of experiments were conducted. The molding experiments determined the relationship of molding conditions to quality after molding, and the relationship of molding conditions to quality after binder removal. The binder removal experiment examined the relationships between pressure and heating rate on the quality of the part. The strength experiment examined the relationship between strength, microstructure, and sintering conditions. Also as part of the specimen development program the cooling pattern of the green injection molded integral shaft spin disk was studied using finite element techniques. This study was conducted in order to determine a cooling method that left no isolated thermal hot zone in the disk. Experience had shown that such a zone caused a void due to shrinkage. The results of the study were presented as temperature contour plots of the disk and die versus time. A program of attachment development was conducted. The integral shaft spin disk required a new attachment design. It is a boreless design; therefore, the tie bolt and Curvic Couplings™ used in previous hot spin testing could not be used. Attachment designs utilizing high expansion plastics to accomodate the difference in thermal expansion between ceramics and metals were developed in bench rigs and the hot spin rig.

U S Army Materials Technology Laboratory
Watertown, Massachusetts 02172-0001
Ceramic Life Prediction
Methodology-Final Report
L R Swank, J A Mangels, J C Conway
and R E Gentile
Research Staff
Ford Motor Company
P O Box 2053
Dearborn, Michigan 48121
Technical Report MTL TR 86-14, May 1986, 43pp.
Illus.-tables, Contract DAAG46-77-C-0078
DOE I No DE-AI03-84GE71411
Final Report January 1983 to December 1985

AD_____
UNCLASSIFIED
UNLIMITED DISTRIBUTION

Key Words

Ceramic materials
Life expectancy
Disks
Test and evaluation
Silicon nitride
Glass ceramics
Gas turbine
Brittle materials design

Fast fracture and stress rupture data were collected on two materials, a sintered silicon nitride and a lithium-aluminum-silicate. The fast fracture data was presented graphically in the form of Weibull plots of percent failed versus failure stress. The stress rupture results were presented in tabular form. Photo-micrographs were presented to illustrate the fracture surfaces of fast fracture and stress rupture failures. A program of specimen development was conducted. The objective of the program was to develop processing techniques to make it possible to fabricate integral shaft spin disks suitable for hot spin testing as stress rupture specimens. The hot spin disk stress rupture results were to be used to correlate experimental time dependent failure results with analytical time dependent failure results. In the specimen development program several sets of experiments were conducted. The molding experiments determined the relationship of molding conditions to quality after molding, and the relationship of molding conditions to quality after binder removal. The binder removal experiment examined the relationships between pressure and heating rate on the quality of the part. The strength experiment examined the relationship between strength, microstructure, and sintering conditions. Also as part of the specimen development program the cooling pattern of the green injection molded integral shaft spin disk was studied using finite element techniques. This study was conducted in order to determine a cooling method that left no isolated thermal hot zone in the disk. Experience had shown that such a zone caused a void due to shrinkage. The results of the study were presented as temperature contour plots of the disk and die versus time. A program of attachment development was conducted. The integral shaft spin disk required a new attachment design. It is a boreless design; therefore, the tie bolt and Curvic Couplings™ used in previous hot spin testing could not be used. Attachment designs utilizing high expansion plastics to accomodate the difference in thermal expansion between ceramics and metals were developed in bench rigs and the hot spin rig.